ATM is a key driver of NF-κB-dependent DNA-damage-induced senescence, stem cell dysfunction and aging

Jing Zhao[1,2,3,*], Lei Zhang[1,2,*], Aiping Lu[4,5], Yingchao Han[7], Debora Colangelo[1,6], Christina Bukata[1], Alex Scibetta[4,5], Matthew J. Yousefzadeh[1,2], Xuesen Li[1], Aditi U. Gurkar[1], Sara J. McGowan[1,2], Luise Angelini[1,2], Ryan O'Kelly[1,2], Hongshuai Li[7], Lana Corbo[1], Tokio Sano[1], Heather Nick[1], Enrico Pola[6], Smitha P.S. Pilla[8], Warren C. Ladiges[8], Nam Vo[7], Johnny Huard[4,5], Laura J. Niedernhofer[1,2], Paul D. Robbins[1,2]

[1]Department of Molecular Medicine and the Center on Aging, Scripps Research, Jupiter, FL 33458, USA
[2]Institute on the Biology of Aging and Metabolism and Department of Biochemistry, Molecular Biology and Biophysics, University of Minnesota Medical School, Minneapolis, MN 55415, USA
[3]Department of Immunology, University of Pittsburgh School of Medicine, Pittsburgh, PA 15261, USA
[4]Department of Orthopaedic Surgery, McGovern Medical School, University of Texas Health Science Center at Houston, Houston, TX 77030, USA
[5]Steadman Philippon Research Institute, Vail, CO 81657, USA
[6]Department of Orthopaedic Surgery, Catholic University of Rome School of Medicine, "A. Gemelli" University Hospital, Roma, Italy
[7]Department of Orthopaedic Surgery, University of Pittsburgh School of Medicine, Pittsburgh, PA 15261, USA
[8]Department of Comparative Medicine, University of Washington, Seattle, WA 98195, USA
*Co-first author

Correspondence to: Paul D. Robbins; email: probbins@umn.edu

ABSTRACT

NF-κB is a transcription factor activated in response to inflammatory, genotoxic and oxidative stress and important for driving senescence and aging. Ataxia-telangiectasia mutated (ATM) kinase, a core component of DNA damage response signaling, activates NF-κB in response to genotoxic and oxidative stress via post-translational modifications. Here we demonstrate that ATM is activated in senescent cells in culture and murine tissues from *Ercc1*-deficient mouse models of accelerated aging, as well as naturally aged mice. Genetic and pharmacologic inhibition of ATM reduced activation of NF-κB and markers of senescence and the senescence-associated secretory phenotype (SASP) in senescent *Ercc1*$^{-/-}$ MEFs. *Ercc1*$^{-/\Delta}$ mice heterozygous for *Atm* have reduced NF-κB activity and cellular senescence, improved function of muscle-derived stem/progenitor cells (MDSPCs) and extended healthspan with reduced age-related pathology especially age-related bone and intervertebral disc pathologies. In addition, treatment of *Ercc1*$^{-/\Delta}$ mice with the ATM inhibitor KU-55933 suppressed markers of senescence and SASP. Taken together, these results demonstrate that the ATM kinase is a major mediator of DNA damage-induced, NF-κB-mediated cellular senescence, stem cell dysfunction and aging and thus, represents a therapeutic target to slow the progression of aging.

INTRODUCTION

With aging there is an inevitable and progressive loss of the ability of tissues to recover from stress, leading to the increased incidence of chronic degenerative diseases. The loss of tissue homeostasis is driven, in part, by an increase in cellular senescence and a decline in stem cell function, resulting in various aging-related diseases, including osteoporosis, intervertebral disc degeneration, chronic kidney disease, diabetes, neurodegeneration and cancer [1–5]. Cellular senescence, characterized by irreversible cell cycle arrest with sustained metabolic activity, is a biological process that is physiologically required during embryonic development, wound healing and tumor suppression [6–10]. Importantly, senescent cells can develop a senescence-associated secretory phenotype (SASP), including expression of IL-6, IL-1α, IL-1β and TNF-α, that affects neighboring cells, disrupts stem cell niches, alters extracellular matrix, and induces secondary senescence [8, 11, 12]. Cellular senescence is mediated by p53/p21 and p16^{INK4a}/retinoblastoma (Rb) tumor suppressor pathways in response to stress [8, 13] conferred by telomere attrition, DNA damage, oxidative and inflammatory stress and oncogene dysregulation [8].

Cellular senescence directly contributes to the progression of aging. For example, depletion of p16^{INK4a} positive cells in both progeroid and naturally aged transgenic mice expressing an inducible apoptotic transgene from the p16^{INK4a} promoter leads to an extension of healthspan [2, 3]. Similarly, clearance of senescent cells using senolytic agents extends healthspan, improves adult stem cell function and extends lifespan in mice [4, 5, 14–17].

The DNA damage response (DDR), essential for genome stability and organismal survival [18–21], is mediated through pathways that recruit multi-protein complexes to sites of DNA double-strand breaks (DSBs) or stalled replication forks. In particular, the MRE11-RAD50-NBS1 (MRN) complex is recruited to sites of DSBs to facilitate the recruitment, retention and activation of the ataxia-telangiectasia mutated (ATM) kinase [22]. Autophosphorylation of ATM at Ser1981 enhances its kinase activity, leading to phosphorylation of histone H2A variant H2AX (γH2AX) in nucleosomes surrounding damaged sites and recruiting more ATM and other repair factors [22, 23]. Additional DDR proteins, including KRAB-associated protein-1 (KAP1), p53 and checkpoint kinase 2 (CHK2), are phosphorylated by ATM kinase, promoting DNA repair, cell-cycle arrest, apoptosis and/or senescence [24, 25].

The Nuclear Factor κB (NF-κB) family of transcription factors consists of five members in mammalian cells, including RelA (p65), RelB, c-Rel,

p50/p105 and p52/p100 [26]. All NF-κB subunits contain a Rel-homology domain (RHD), which is essential for DNA binding activity and dimerization. NF-κB functions to regulate innate and adaptive immune responses, embryonic development, proliferation, apoptosis, oncogenesis and senescence [26]. The canonical NF-κB pathway is activated by inflammatory stimuli, such as TNF-α, IL-1β and LPS, which lead to the activation of the IκB kinase (IKK). IKK is composed of two catalytic subunits, IKKα and IKKβ, and one regulatory subunit, NF-κB essential modifier (NEMO) or IKKγ [26]. Activated IKK complex phosphorylates the inhibitory protein IκBα to facilitate its polyubiquitination and degradation by the 26S proteasome, resulting in the translocation of the NF-κB heterodimer into the nucleus where it regulates gene transcription [26]. In addition, genotoxic stress activates a TNF-α-independent, but ATM-dependent NF-κB pathway via nuclear-localized NEMO [27, 28]. ATM phosphorylates NEMO at Ser85, which in turn induces sumoylation and mono-ubiquitination of NEMO at Lys277 and 309 [29]. These post-translational modifications eventually lead to the nuclear export of the ATM-NEMO complex to the cytoplasm where it associates with ubiquitin and SUMO-1 modified RIP1 and TAK1, activating the catalytic IKKβ subunit [28, 30].

NF-κB activity increases in multiple tissues of humans and rodents with aging and promotes cellular senescence [31–36]. Genetic depletion of RelA/p65 in aged mouse skin and a mouse model of human progeroid syndrome, reversed gene expression signature of aging and aging phenotypes [35, 37]. In addition, heterozygosity of p65/RelA in a mouse model of Hutchinson-Gilford Progeria Syndrome (*Zmpste24*$^{-/-}$) resulted in attenuated aging pathology and a prolonged lifespan, linked in part to a reduced systemic inflammatory response and a reduction in ATM/NEMO-mediated NF-κB activation [34]. In addition, Nfkb1$^{-/-}$ (p50$^{-/-}$) mice have increased low-grade inflammation with signs of premature aging, including neural degeneration, impaired regeneration and declined overall lifespan [38–41]. Activation of NF-κB also is associated with multiple aging-related chronic diseases, including Alzheimer's disease, Parkinson's disease, Type II diabetes, osteoporosis and atherosclerosis [42], possibly through an increase in secretion of SASP factors [43].

DNA damage is known to increase with aging as demonstrated by an increase in DNA damage foci (γH2AX) and oxidative DNA lesions (8,5'-cyclopurines) [44, 45]. Intriguingly, persistent DDR signaling mediated by ATM activation has been reported to contribute to cellular senescence and SASP [46]. *In vitro*, SASP is dependent on ATM activation,

suggesting a molecular link between ATM and NF-κB [8, 46, 47]. However, it is still unclear if aberrant DNA damage-induced activation of ATM *in vivo* exacerbates the cellular stress response to increase NF-κB, senescence, SASP and subsequently aging.

To address the role of ATM in driving NF-κB mediated senescence and aging, we used *Ercc1^{-/Δ}* mice that model a human progeroid syndrome caused by impaired repair of DNA damage. The mice express only 5% of the normal level of the DNA repair endonuclease ERCC1-XPF that is required for nucleotide excision, interstrand crosslink and repair of some double-strand breaks. As a consequence, the *Ercc1^{-/Δ}* mice spontaneously and rapidly develop progressive age-related diseases, including osteoporosis, sarcopenia, intervertebral disc degeneration, glomerulonephropathy, neurodegeneration, peripheral neuropathy and loss of cognition [48].

Here, we demonstrate that ATM and downstream effectors are persistently elevated in *Ercc1^{-/Δ}* and naturally aged mice, concomitant with hyperactive NF-κB signaling. Reducing ATM activity either genetically or pharmacologically reduced cellular senescence and downregulated NF-κB activation in cell culture. Importantly, *Ercc1^{-/Δ}* mice heterozygous for *Atm* exhibited significantly reduced NF-κB activity, reduced cellular senescence, improved muscle-derived stem/progenitor cell function and attenuated age-related bone and intervertebral disc pathologies, leading to an extension of healthspan. Similarly, inhibiting ATM in *Ercc1^{-/Δ}* mice by treatment with the ATM inhibitor KU-55933 reduced senescence and SASP marker expression. These results demonstrate a key role for ATM in aging and suggest that it is a therapeutic target for delaying or improving numerous age-related diseases.

RESULTS

NF-κB and ATM signaling are highly activated in cellular senescence, as well as accelerated and natural aging

Our previous studies using transgenic mice carrying a NF-κB-dependent EGFP reporter demonstrated an increase in the percentage of EGFP-positive cells in the liver, kidney, skeletal muscle and pancreas of progeroid *Ercc1^{-/Δ}* and aged wild-type (WT) mice [35]. To further quantify NF-κB activation with aging, p-p65 (Ser536), a marker of NF-κB activation, was measured in murine liver (Figure 1A). Phosphorylation of p65 was significantly increased in 16-week-old *Ercc1^{-/Δ}* mice compared to age-matched WT mice (Supplementary Figure 1A). In addition, there was an increase in the level of p-ATM as well as two senescence markers, γH2AX [49] and p21, in *Ercc1^{-/Δ}* liver compared to WT

controls (Figure 1B and Supplementary Figure 1B). To determine if NF-κB and ATM were activated in WT mice with aging, p-p65, p-IκBα and p-ATM were measured by immunoblot in liver extracts from WT mice at multiple ages. The levels of p-p65 and p-IκBα increased gradually with age from 3 to 12 and 24-months of age (Figure 1C and Supplementary Figure 1C). These correlated with increased levels of p-ATM and the senescence marker p21 at 12 and 24 months of age (Figure 1D and Supplementary Figure 1D).

To examine ATM and NF-κB activation with senescence, the phosphorylation of ATM and NF-κB targets were measured initially in primary *Ercc1^{-/-}* mouse embryonic fibroblasts (MEFs), which undergo premature senescence at 20% O_2. The levels of p-ATM and p-KAP1 were increased in *Ercc1^{-/-}* MEFs compared to WT MEFs (Figure 1E). Moreover, p-p65 levels were increased in passage 5 *Ercc1^{-/-}* MEFs compared to WT cells (Figure 1F). There also was an increase in nuclear staining of p65 and NEMO in *Ercc1^{-/-}* MEFs compared to WT cells, indicating NF-κB activation through a NEMO-dependent manner (Figure 1G). These findings suggest that NF-κB and ATM are co-activated in cells and tissues with higher levels of DNA damage-induced senescence.

Pharmacologic inhibition of ATM rescues senescence caused by genotoxic stress via suppressing NEMO-dependent NF-κB activation

To elucidate further the causative role of activated ATM and DDR signaling in driving senescence, the effect of a selective ATM kinase inhibitor, KU-55933 [50], on senescence in MEFs was examined. Treatment of DNA repair deficient *Ercc1^{-/-}* MEFs with KU-55933 (10 μM) reduced the percent of SA-βgal positive cells to a level similar to WT MEFs (Figure 2A and 2B). Additional markers of senescence, including the cell-cycle regulators p21^{Cip1} and p16^{INK4A}, also were decreased by KU-55933 treatment (Figure 2C). As expected, autophosphorylation of ATM at Ser1981 was downregulated by the ATM inhibitor, as were the levels of p-KAP1 and γH2AX (Figure 2D). Interestingly, ATM inhibition also decreased Poly [ADP-ribose] polymerase 1 (PARP1) abundance (Figure 2D), an enzyme that promotes DNA repair and chromatin remodeling, utilizing NAD^+ as a cofactor [51]. Interestingly, our results also suggest that inhibition of ATM activity may regulate ATM expression at protein level as indicated by reduced ATM level (Figure 2D). Furthermore, ATM inhibition reduced the abundance of nuclear-localized p65 and NEMO and the level of p-p65 (Figure 2E), as well as NF-κB transcriptional activity, measured using a NF-κB luciferase reporter assay (Figure 2F). Finally, treatment with the ATM inhibitor significantly reduced expression

of multiple senescence and SASP markers as determined by qRT-PCR (Figure 2G). Taken together, these results suggest that ATM activation triggered by endogenous DNA damage plays a critical role in driving cellular senescence, SASP and NF-κB activation in a NEMO-dependent manner.

Genetic depletion of Atm decreases genotoxic stress-induced cellular senescence

To eliminate possible off-target effects of the ATM inhibitor KU-55933, $Ercc1^{-/-}$ MEFs heterozygous for Atm ($Ercc1^{-/-}Atm^{+/-}$) were generated. The $Ercc1^{-/-}Atm^{+/-}$
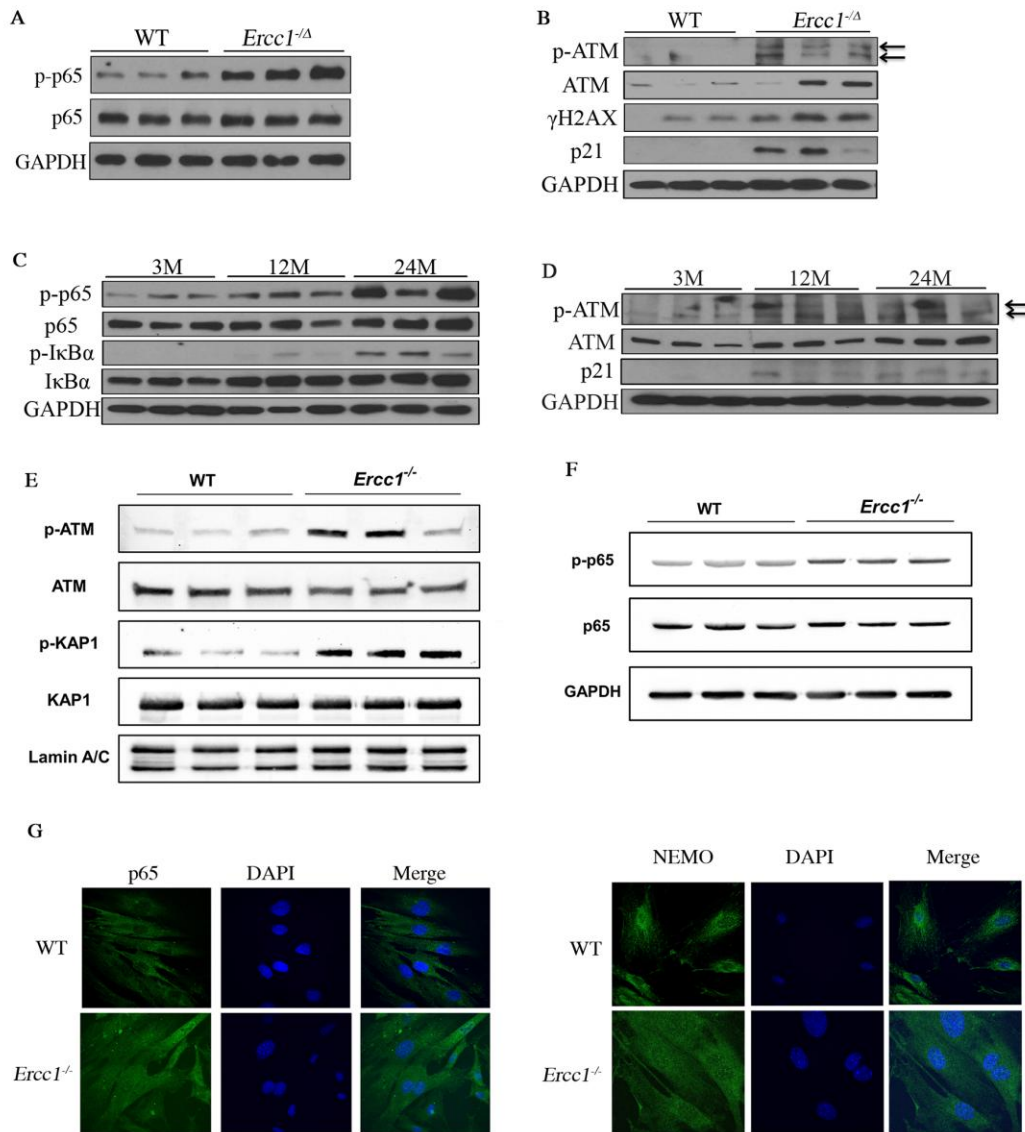
Figure 1. DDR and NF-κB are activated concomitantly in senescent MEFs and aged tissues. (**A**) Immunoblot detection of p-p65 and total p65 in liver tissue from 16-week-old WT (n=3) and $Ercc1^{-/\Delta}$ (n=3) mice. (**B**) Immunoblot detection of phosphorylation of ATM and downstream targets γH2AX and p21 in liver from 16-week-old WT and $Ercc1^{-/\Delta}$ mice. (**C**) Immunoblot detection of phosphorylation of NF-κB and IκBα in liver lysates from 3, 12 and 24 month-old WT mice. n=3 mice per group. (**D**) Immunoblot detection of p-ATM, ATM and p21 in the same liver lysates. (**E**) Immunoblot detection of DDR effectors in nuclear extracts from passage 5 WT and Ercc1$^{-/-}$ MEFs, grown at 20% oxygen. (**F**) Level of NF-κB activation is higher in $Ercc1^{-/-}$ MEFs compared to WT MEFs at passage 5, as measured by Immunoblot detection of p-p65 and total p65 in WT and $Ercc1^{-/-}$ MEFs at passage 5 after culturing in 20% oxygen. (**G**) Representative images of immunofluorescent detection of p65 and NEMO in passage 4 WT and $Ercc1^{-/-}$ MEFs grown at 20% oxygen. Blue: DAPI staining; Green: p65 (top panel) or NEMO (bottom panel). Images were taken at the magnification of 60x.
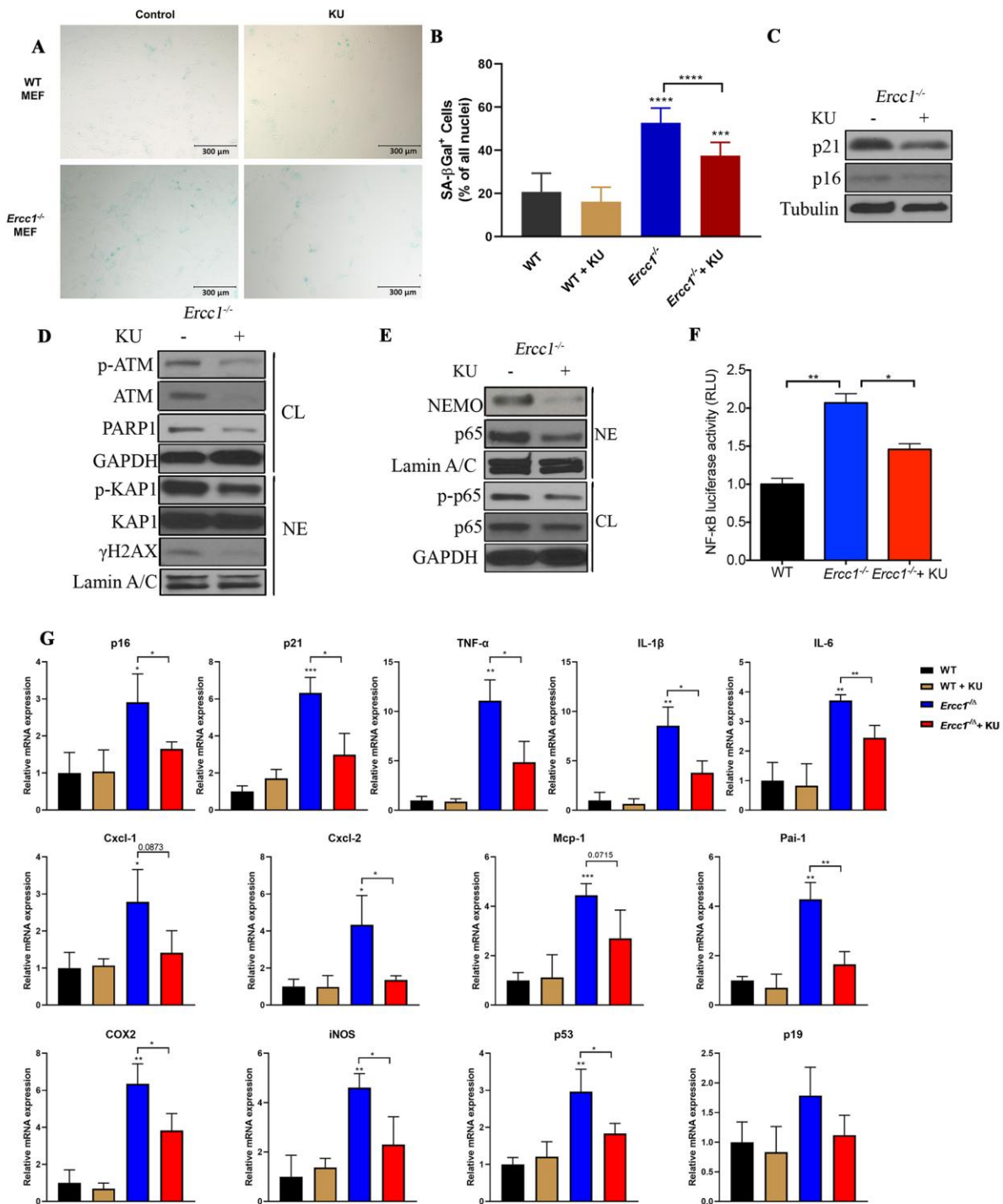
Figure 2. Pharmacologic inhibition of ATM rescues oxidative stress-induced senescence by suppressing ATM- and NEMO-mediated NF-κB activation. (**A**) Representative images of primary WT and *Ercc1*-/- MEFs were induced to undergo senescence by serial passaging at 20% oxygen. At passage 5, MEFs were grown in the presence or absence of KU-55933 (10 µM) for 72 hrs. Senescence was determined by SA-βgal staining. Images were obtained at the magnification of 10x. (**B**) Quantitation of the percent SA-βgal positive cells. Graph represents the mean +/- s.e.m. of three independent experiments. Student's t-test, ***p <0.001, ****p <0.0001. (**C**) Passage 5 *Ercc1*-/- MEFs treated with vehicle or KU-55933 (10 µM) for 72 hours were collected and levels of p21 and p16[INK4a] were determined by western blotting. (**D**) Passage 5 *Ercc1*-/- MEFs were treated with KU-55933 (10 µM) for 72 hours and whole cell lysate (CL) and nuclear extracts (NE) were analyzed by immunoblotting for expression of proteins involved in the DNA damage response. (**E**) Whole cell lysate (CL) and nuclear

extract (NE) were extracted from *Ercc1⁻/⁻* MEFs treated with 10 µM of KU-55933 for analysis of nuclear NEMO and p65. GAPDH was used as a loading control of total proteins and LaminA/C as a loading control of nuclear protein. (**F**) Passage 5 WT and *Ercc1⁻/⁻* MEFs transfected with a NF-κB-luciferase reporter construct were cultured in the presence or absence of KU-55933 (10 µM) and were collected for luciferase assays after 72 hours. (**G**) qRT-PCR analysis of mRNA expression in passage 5 WT and *Ercc1⁻/⁻* MEFs treated with or without of KU-55933 (10 µM) for 72 hrs. P values were determined using a Student's t-test. *p<0.05, **p<0.01, ***p <0.001.

MEFs had increased proliferation compared to *Ercc1⁻/⁻* MEFs (Figure 3A). There also was a reduction in the percent of SA-ßgal⁺ *Ercc1⁻/⁻Atm⁺/⁻* MEFs compared to *Ercc1⁻/⁻* MEFs (Figure 3B and 3C). Expression of *p16ᴵᴺᴷ⁴ᵃ* also was reduced in the double mutant MEFs (Figure 3D). Finally, there was a reduction in the level of secreted IL-6, a SASP factor, in conditioned media from *Ercc1⁻/⁻Atm⁺/⁻* MEFs compared to *Ercc1⁻/⁻* cells (Figure 3E). Taken together, these results suggest that ATM promotes genotoxic stress-induced cellular senescence, in part, through the activation NF-κB signaling.

Genetic depletion of Atm extends healthspan in *Ercc1⁻/Δ* mice by reducing cellular senescence

To determine if *Atm* heterozygosity extends healthspan in *Ercc1⁻/Δ* mice, age-related symptoms, including kyphosis, tremor, ataxia, gait disorder, hind limb muscle wasting, forelimb grip strength and, in particular, dystonia were measured weekly in *Ercc1⁻/Δ* and *Ercc1⁻/ΔAtm⁺/⁻* mice. As shown in Figure 4A and 4B, *Atm* heterozygosity reduced the severity and slowed progression of aging symptoms in *Ercc1⁻/Δ* mice.

To determine if the extended healthspan correlated with reduced cellular senescence in *Ercc1⁻/ΔAtm⁺/⁻* mice, the levels of expression of senescent markers and SASP factors were measured by qRT-PCR analysis. Expression of p21 was significantly reduced in 12-week-old *Ercc1⁻/ΔAtm⁺/⁻* livers compared to those from aged-matched *Ercc1⁻/Δ* mice, as was IL-6, a SASP factor and NF-κB target gene (Figure 4C). Similarly, the expression of senescence markers and SASP factors (except p16) were significantly reduced in *Ercc1⁻/ΔAtm⁺/⁻*
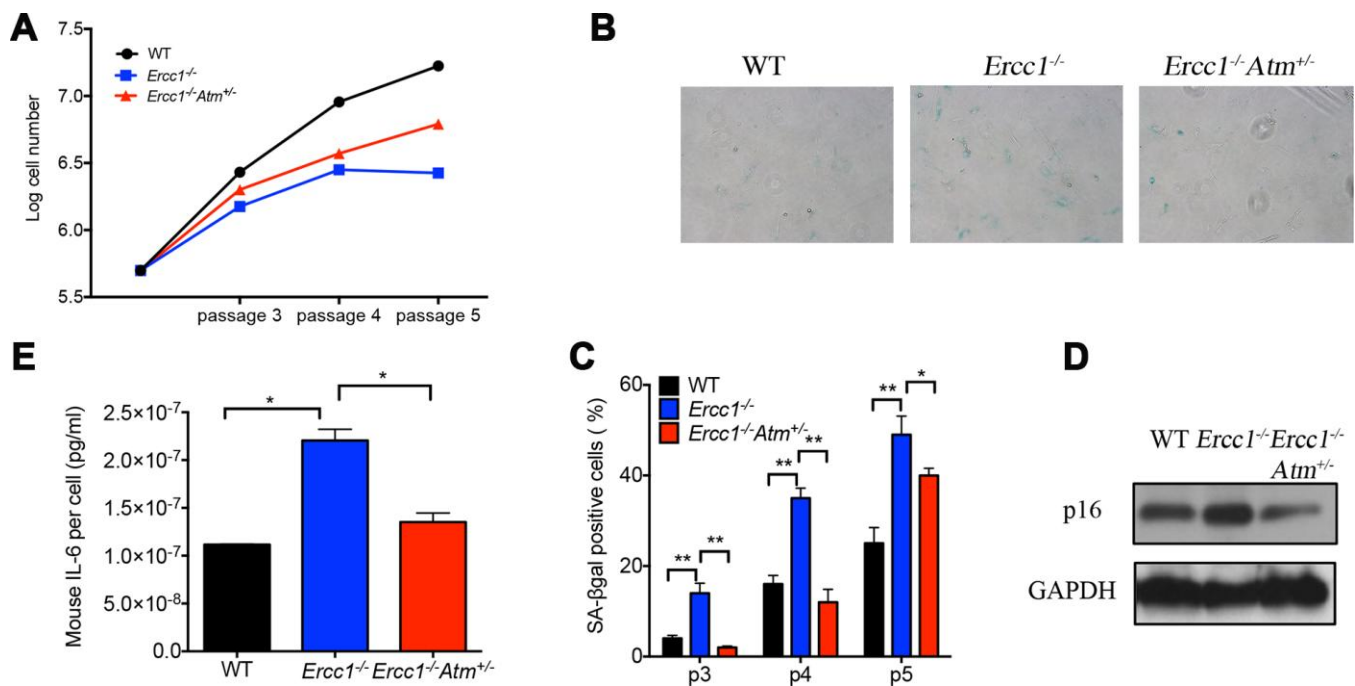

Figure 3. Oxidative stress-induced cellular senescence is reduced by genetic depletion of *Atm*. (**A**) Proliferation of WT (black), *Ercc1⁻/⁻* (blue) and *Ercc1⁻/⁻Atm⁺/⁻* (red) MEFs serially passaged at 20% oxygen was measured by an automated cell counter. Data shown are representative of three independent experiments using distinct MEF lines. (**B**) SA-βgal staining of serially passaged MEFs cultured at 20% oxygen. Shown are representative images of passage 5 WT, *Ercc1⁻/⁻* and *Ercc1⁻/⁻Atm⁺/⁻* MEFs taken at 10x magnification. (**C**) The average percentage of SA-βgal positive cells at each indicated passage. Ten fields were acquired and quantified per sample. Data shown are representative of two independent experiments. (**D**) Senescent WT, *Ercc1⁻/⁻* and *Ercc1⁻/⁻Atm⁺/⁻* MEFs (passage 5) cultured at 20% oxygen for 72 hrs were collected and lysed for immunoblot analysis of p16ᴵᴺᴷ⁴ᵃ. (**E**) Supernatant collected from senescent WT, *Ercc1⁻/⁻* and *Ercc1⁻/⁻*Atm⁺/⁻ MEFs was analyzed by ELISA for secreted IL-6. Graphs represent mean+/- s.e.m. P value was determined using Student's t-test. *p<0.05, **p<0.01.

quadriceps compared with those in *Ercc1*$^{-/\Delta}$ mice (Figure 4D). In wildtype mice, there was no effect of ATM heterozygosity on expression of these senescence and SASP markers. Interestingly, IL-6 and TNF-α, but not p21^{Cip1} or p16^{INK4a} expression, were significantly lower in liver of 12-week-old *Ercc1*$^{-/\Delta}$ *p65*$^{+/-}$ mice compared to age-matched *Ercc1*$^{-/\Delta}$*Atm*$^{+/-}$ mice (Figure 4E). This indicates a distinct role for NF-κB in promoting aging. Taken together, these results suggest that genetic reduction of ATM leads to a reduction in cellular senescence and aging symptoms *in vivo*.

To determine if pharmacologic inhibition of ATM in *Ercc1*$^{-/\Delta}$ mice confers a similar reduction in senescence and SASP markers as ATM heterozygosity, *Ercc1*$^{-/\Delta}$ mice were treated three times per week i.p. for 2 weeks with 10 mg/kg of KU-55933. The mice were then analyzed for the extent of senescence and SASP in different tissues. As shown in Figure 4F, the levels of expression of senescent markers and SASP factors were measured were significantly reduced in liver tissues from *Ercc1*$^{-/\Delta}$ mice compared to untreated controls.

Atm haploinsufficiency improves function of muscle-derived stem/progenitor cells (MDSPC)

A decline in stem cell function has long been associated with aging, which in the musculoskeletal system leads to sarcopenia and muscle wasting [1, 52]. We previously reported that muscle-derived stem/progenitor cells (MDSPCs) isolated from *Ercc1*$^{-/\Delta}$ mice failed to proliferate or differentiate properly, similar to MDSCPs from naturally aged mice [53]. Interestingly, the function of MDSPCs isolated from *Ercc1*$^{-/\Delta}$ mice was partially restored by *Atm* heterozygosity (Figure 5). In fact, MDSPCs isolated from *Ercc1*$^{-/\Delta}$*Atm*$^{+/-}$ mice showed similar levels of myogenic differentiation to WT mice (Figure 5A, 5C and 5D). Proliferation of MDSPCs isolated from *Ercc1*$^{-/\Delta}$*Atm*$^{+/-}$ mice also increased by 50% compared to control MDSPCs (Figure 5B). This result is consistent with delayed onset and reduced severity of gait disorder observed in *Ercc1*$^{-/\Delta}$*Atm*$^{+/-}$ mice, which is partly due to severe muscle wasting (data not shown).

Atm haploinsufficiency improves aging-related pathology in certain tissues

To further assess the effect of ATM status on aging, tissues from 12-week *Ercc1*$^{-/\Delta}$ and *Ercc1*$^{-/\Delta}$*Atm*$^{+/-}$ mice were examined histologically. There are reduced lymphoid aggregates in the liver and kidney of *Ercc1*$^{-/\Delta}$ and *Ercc1*$^{-/\Delta}$*Atm*$^{+/-}$ mice, suggesting reduced inflammatory infiltration in tissues at the age analyzed [54]. In addition, *Ercc1*$^{-/\Delta}$*Atm*$^{+/-}$ mice had reduced age-related bony changes in the lumbar vertebrae, as

determined using μCT. Compared to WT mice, *Ercc1*$^{-/\Delta}$ mice showed marked trabecular bone loss (Figure 6A), signified by an increase in osteoporosis (1-BV/TV), a decrease in trabecular number (Tb.N) and trabecular thickness (Tb.Th) and an increase in the trabecular spacing (Tb.Sp). *Atm* heterozygosity significantly improved bone qualities when compared with *Ercc1*$^{-/\Delta}$ mice, showing reduced vertebral osteoporosis and trabecular spacing, accompanied by a significant increase in trabecular number (Figure 6A). However, no significant difference was found in trabecular thickness (Figure 6A). *Ercc1*$^{-/\Delta}$*Atm*$^{+/-}$ mice also had improved Safranin O staining of the intervertebral disc from the lumbar spines, consistent with significantly higher levels of glycosaminoglycans (GAGs) in the nucleus pulposus (Figure 6B and 6C) [55–57]. GAG measurement indicates the level of the matrix proteoglycans, which plays a critical role in counteracting mechanical forces imparted on the spine [58]. Taken together, these results suggest that heterozygosity of *Atm* improves certain age-related conditions, in particular in the musculoskeletal system.

Atm haploinsufficiency reduces NF-κB signaling in Ercc1$^{-/\Delta}$ mice

To determine the extent to which ATM signaling mediates NF-κB activation *in vivo*, livers from 12- and 16-week-old *Ercc1*$^{-/\Delta}$ and *Ercc1*$^{-/\Delta}$*Atm*$^{+/-}$ mice were examined. There was a significant decrease in DDR signaling in *Ercc1*$^{-/\Delta}$*Atm*$^{+/-}$ mice compared to *Ercc1*$^{-/\Delta}$ mice as indicated by reduced levels of p-ATM and γH2AX (Figure 7A, 7C and Supplementary Figure 2A, 2C). Moreover, the levels of p21^{Cip1} were significantly decreased in livers from *Ercc1*$^{-/\Delta}$*Atm*$^{+/-}$ mice, particularly at 12 weeks of age, consistent with reduced cellular senescence and the qRT-PCR results (Figure 4C). Importantly, the level of phospho-p65 was greatly reduced in *Ercc1*$^{-/\Delta}$*Atm*$^{+/-}$ livers (Figure 7B, 7D and Supplementary Figure 2B, 2D), suggesting that NF-κB activation in *Ercc1*$^{-/\Delta}$ mice is driven, at least in part, by ATM activation. Accordingly, there was reduced p-IκBα and IκBα levels in *Ercc1*$^{-/\Delta}$*Atm*$^{+/-}$ mice compared to *Ercc1*$^{-/\Delta}$ controls (Figure 7B, 7D and Supplementary Figure 2B, 2D) [59, 60].

To determine if the molecular changes in *Ercc1*$^{-/\Delta}$*Atm*$^{+/-}$ mice mirror that in *Ercc1*$^{-/\Delta}$*p65*$^{+/-}$ mice, ATM and NF-κB activation was measured in *Ercc1*$^{-/\Delta}$ and *Ercc1*$^{-/\Delta}$*p65*$^{+/-}$ mice. There was no difference in the level of ATM or p-ATM between *Ercc1*$^{-/\Delta}$*p65*$^{+/-}$ and *Ercc1*$^{-/\Delta}$ mice (Figure 7E and Supplementary Figure 2E), suggesting that DDR/ATM signaling is the upstream regulator of NF-κB. The levels of p-p65 and total IκBα were reduced in *Ercc1*$^{-/\Delta}$*p65*$^{+/-}$ mice compared to *Ercc1*$^{-/\Delta}$ mice (Figure 7F and Supplementary Figure 2F),
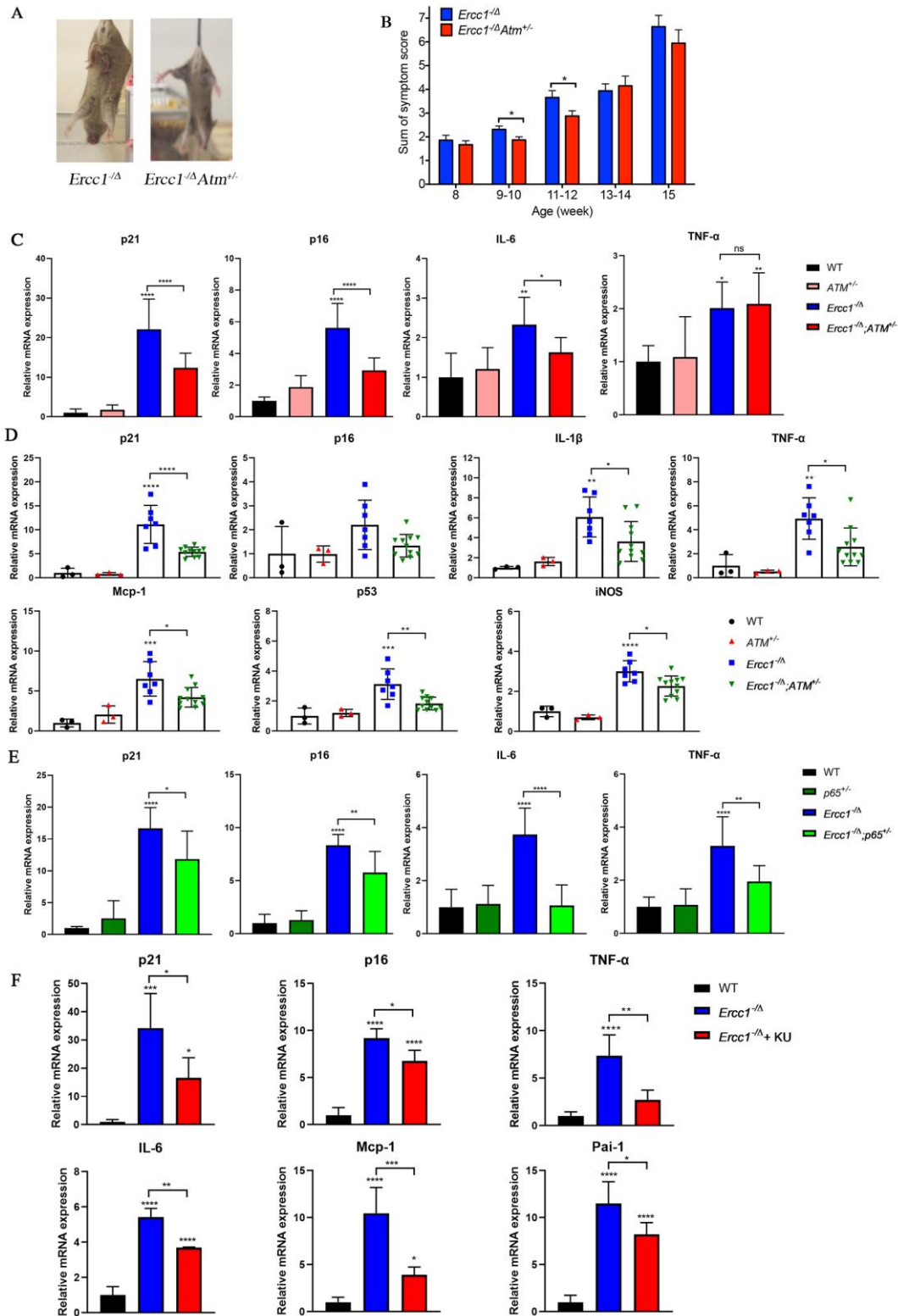
Figure 4. Genetic reduction of *Atm* attenuates aging phenotypes and reduces cellular senescence *in vivo*. (**A**) Representative images (left panel) of 15-week-old *Ercc1*$^{-/Δ}$ and *Ercc1*$^{-/Δ}Atm^{+/-}$ mice illustrating the severity of their dystonia. (**B**) The composite score of aging symptoms (right panel) was plotted at the indicated ages. n=8-10 mice per group. (**C**) qRT-PCR analysis of mRNA expression in liver from 12-week-old WT, *Atm*$^{+/-}$, *Ercc1*$^{-/Δ}$ and *Ercc1*$^{-/Δ}Atm^{+/-}$ mice. n=3-6 per group. (**D**) qRT-PCR analysis of mRNA expression in quadriceps from 12-

consistent with qRT-PCR results (Figure 4E) showing reduced NF-κB-mediated transcription. Taken together, these results suggest that DDR signaling plays an essential role in NF-κB activation in response to endogenous DNA damage. Moreover, the deletion of one *Atm* allele is sufficient to attenuate DDR signaling and dampen NF-κB activation *in vivo*.

DISCUSSION

DNA damage is a critical factor in driving cellular senescence and aging [61]. Multiple human diseases of accelerated aging, such as XFE progeroid syndrome, Cockayne syndrome, Hutchinson-Gilford progeria and Werner syndrome are caused by inherited defects in maintaining genome integrity [48, 62]. Levels of oxidative DNA damage are increased in old or progeroid

organisms compared to young [44, 63, 64]. Although the ATM kinase is a critical mediator of the DNA damage response, *in vivo* evidence linking chronic activation of ATM to senescence and aging is still lacking. Here, we demonstrate that ATM activation increases with aging in mammals. In addition, in the *Ercc1*[-/Δ] progeroid mouse model of accelerated aging, genetic reduction of ATM reduces cellular senescence, improves stem cell function, extends healthspan and reduces certain age-related pathologies in the musculoskeletal system. Moreover, we demonstrate that ATM promotes senescence and aging, at least in part, by regulating the transcriptional activity of NF-κB (Figure 8).

ATM activity is increased in liver with aging in not only progeroid *Ercc1*[-/Δ] mice, but also naturally aged WT mice. Similarly, there was an increase in NF-κB activity
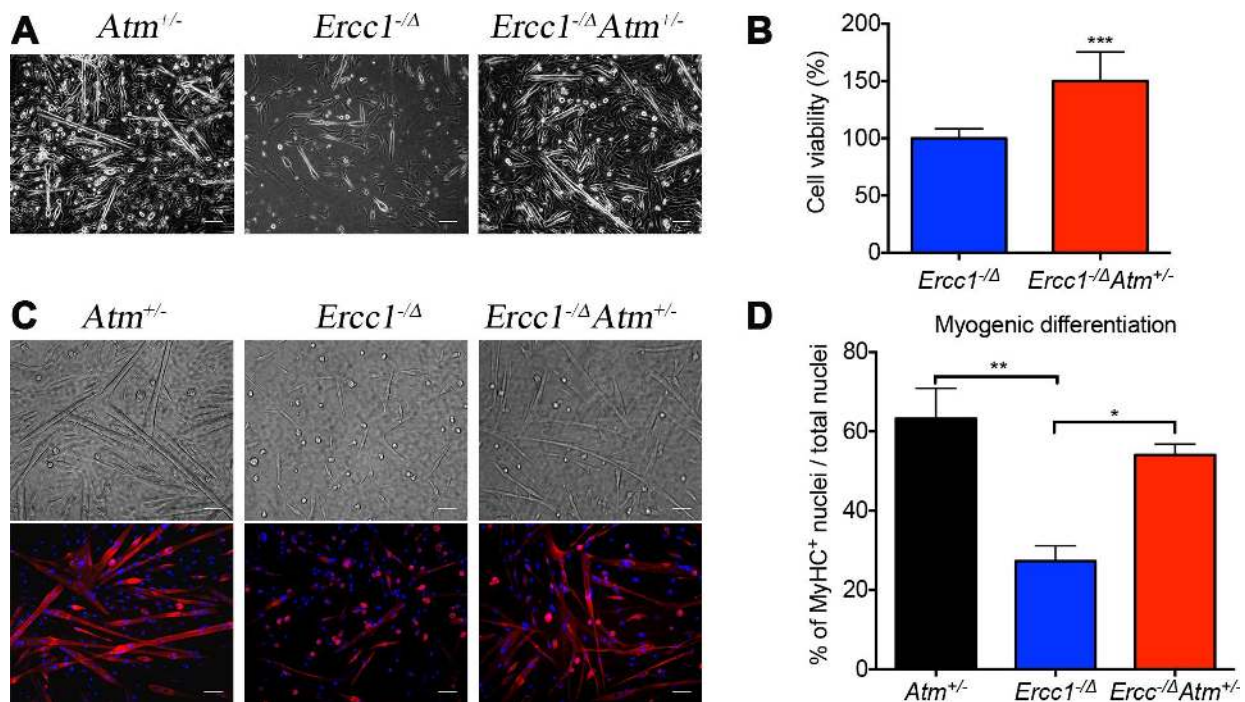

Figure 5. *Atm* heterozygosity improves muscle stem cell function and muscle regeneration. Myogenic progenitor cells (myoblasts) and MDSPCs were isolated via preplate technique, 3 days after myoblasts were obtained, and the bright field pictures were taken. A total of three populations of *Atm*^{+/-}, *Ercc1*[-/Δ]*Atm*^{+/-} and *Ercc1*[-/Δ] were isolated from distinct mice and tested. All scale bars = 100 μm. (**A**) MDSPCs were cultured in myogenic differentiation medium for 3 days. Bright field images were taken and the cell fusion into multinucleated myotubes was determined by immuno-staining for MyHCf, a terminal myogenic differentiation marker. (**B**) Cell proliferation of MDSPCs was measured using an MTS assay. The graph displays the average of three populations. Error bars indicate mean ± SD. ***P<0.001 (**C**) Representative images of immunofluorescence detection of differentiated myofibers. All scale bars in panel C=50 μm. (**D**) Myogenic differentiation was quantified by determining the number of nuclei in MyHCf positive myotubes relative to the total number of nuclei in the culture. Error bars indicate "mean ±SD". *P<0.05. **P<0.01. Error bars indicate "mean ± SD". *P<0.05. Two-tailed Student's t-test was performed.

in livers that correlates with ATM activity. Conversely, a reduction in ATM activation *in vivo* either genetically or pharmacologically resulted in a reduction in the levels of γH2AX in liver and decreased expression of senescent markers and SASP, in particular *p21^Cip1* and *Il6* (Figure 4C and 7A, 7C). Consistent with these observations, there was an increase in ATM and NF-κB activity in ERCC1-deficient cells grown under oxidative stress conditions in cell culture. Reduction of ATM either genetically or pharmacologically in MEFs also resulted in a reduction in oxidative stress-induced senescence along with reduction in NF-κB activation.

We previously demonstrated that heterozygosity in p65/RelA (*Ercc1^-/Δ^p65^+/-*) in *Ercc1^-/Δ* mice resulted in reduced senescence in multiple tissues as well as extended healthspan. Here we demonstrate that *Atm*

heterozygosity reduced NF-κB activation to an extent similar to p65 heterozygosity in *Ercc1^-/Δ* mice, suggesting that ATM kinase is a major activator of NF-κB in the context of DNA-damage mediated senescence and aging. As a result, expression of SASP factors transcriptionally regulated by NF-κB, especially IL-6, was down-regulated in livers of both *Ercc1^-/Δ^p65^+/-* and *Ercc1^-/Δ^Atm^+/-* mice. These findings support previous studies reporting that ATM activation is indispensable for the SASP phenotype secreting inflammatory cytokines [46, 65]. Interestingly, p65/RelA heterozygosity resulted in a stronger reduction in IL-6 and TNF-α expression compared to *Atm* heterozygosity, suggesting either an ATM-independent pathway or that heterozygosity of *Atm* has less of an effect on the pathway. We speculate that DSBs activate NF-κB primarily through an ATM/NEMO-dependent pathway,
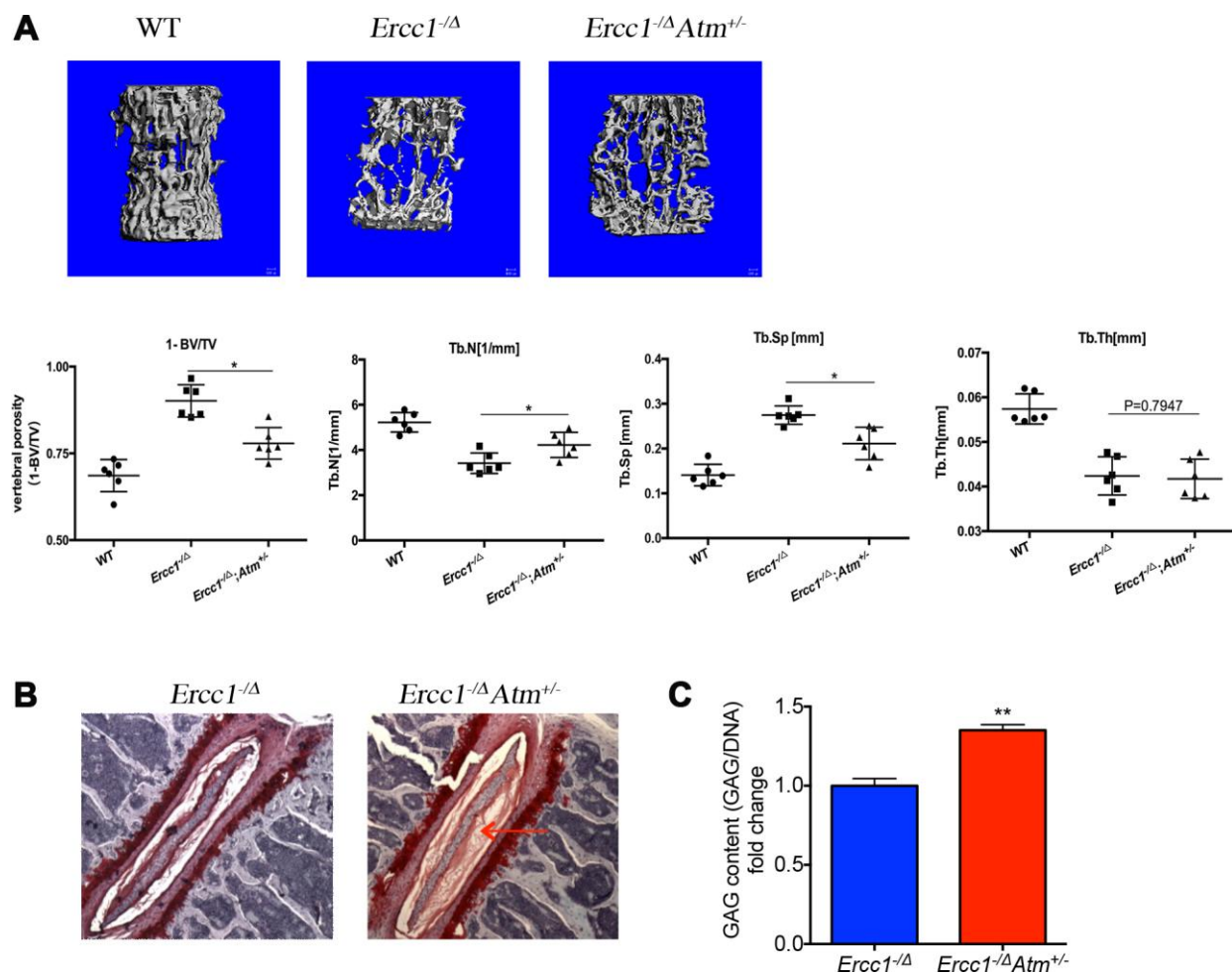

Figure 6. Genetic reduction of *Atm* improves bone and intervertebral disc pathology in progeroid *Ercc1^-/Δ* mice. (**A**) Representative micro-CT images of lumber spines comparing severity of osteoporosis in 16-week-old WT, *Ercc1^-/Δ*, *Ercc1^-/Δ^Atm^+/-* mice. n=3-5 per group. Quantification of vertebral porosity, trabecular number, trabecular separation, thickness of trabecular bone was performed and shown. (**B**) Safranin O staining for disc matrix in thoracic discs from 12-week-old *Ercc1^-/Δ* and *Ercc1^-/Δ^Atm^+/-* mice. (**C**) GAG content measured by DMMB assays with NP tissues isolated from 12-week-old lumber discs. n=3 each group. Mean+/- s.e.m. P value was determined using Student's t-test. **p<0.01.

which then increases the production of TNF-α and other SASP factors. These SASP factors, in turn, trigger a second wave of NF-κB activation, enhancing cell-autonomous and cell-non-autonomous senescence [30, 66] (Figure 8). Thus, *Atm* haploinsufficiency only dampens the primary activation of NF-κB, while p65 heterozygosity targets both primary and secondary NF-κB activation, conferring a stronger inhibition of the SASP phenotype. These results also are consistent with a greater effect of heterozygosity in p65/RelA on liver and kidney pathology than *Atm* heterozygosity.

We previously reported that reduction in p65/RelA in muscle derived stem/progenitor cells (MDSPCs) from *Ercc1*$^{-/\Delta}$ mice improved their ability to proliferate as well as differentiate. Here we demonstrated that reduction in ATM activity also improved self-renewal

and differentiation in muscle derived stem/progenitor cells, suggesting persistent activation of ATM-dependent signaling negatively regulates stem cell function (Figure 5). This consistent with the previous observation that depletion of p21^{Cip1}, which is regulated by ATM-p53, restores stem cell self-renewal and tissue homeostasis without accelerating carcinogenesis in mice deficient in telomerase [67].

Moreover, we and others previously demonstrated that genetic and pharmacological reduction in p65/RelA improves bone architecture and reduces osteoporosis [34, 35]. Here we demonstrated that *Atm* haploinsufficiency also leads to significantly improved osteoporosis and reduced disc degeneration (Figure 6), suggesting ATM activation could contribute to increased chronic inflammation in spines via activating NF-κB in aging.
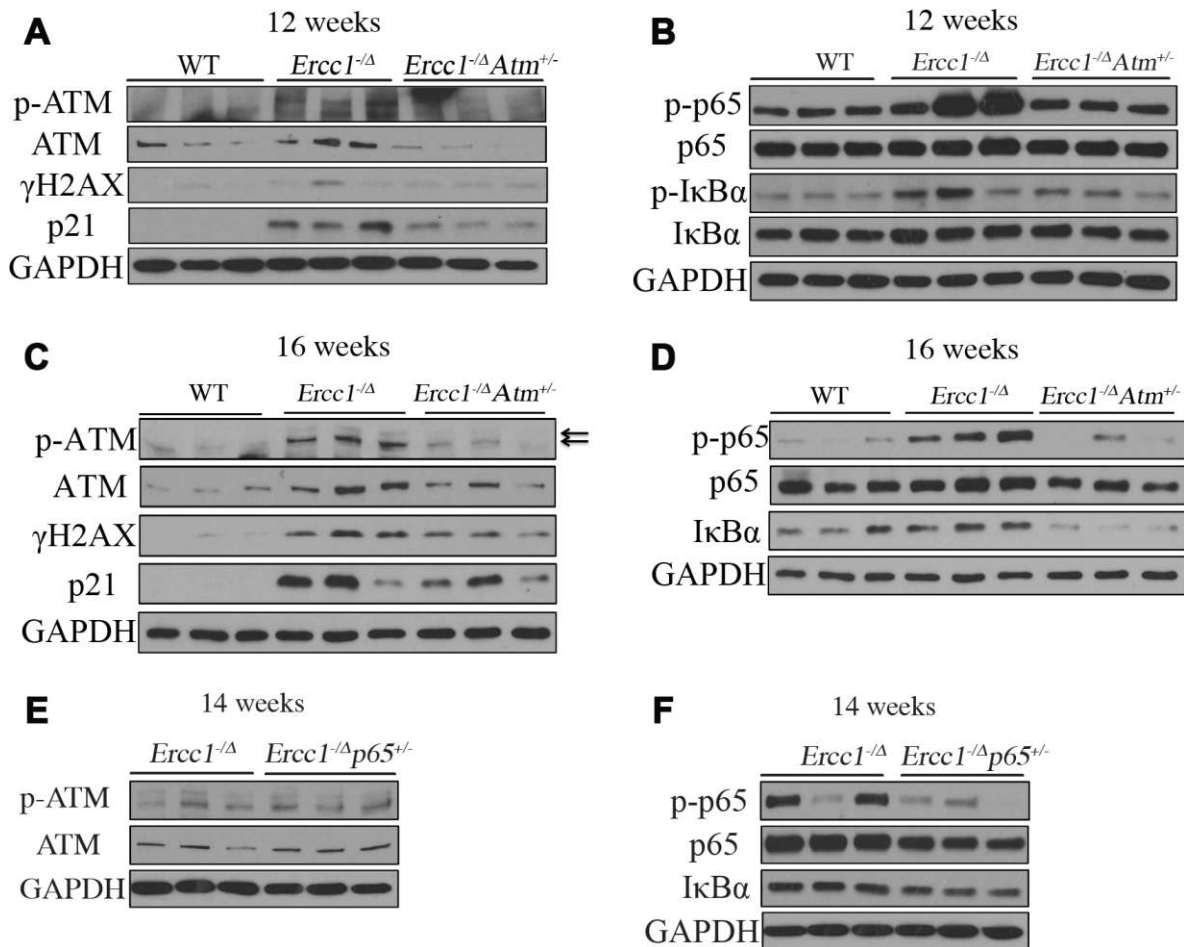

Figure 7. ATM and NF-κB activation are downregulated in *Ercc1*$^{-/\Delta}$ mice heterozygous for *Atm*. (**A**) Livers were collected at 12 weeks of age from WT, *Ercc1*$^{-/\Delta}$ and *Ercc1*$^{-/\Delta}$Atm$^{+/-}$ mic (n=3 per genotype) and lysates analyzed by western blot for activation of ATM and its downstream effectors. (**B**) Same liver lysates were used to measure phosphorylation of p65 and IκBα. (**C**) Western blot analysis of livers from 16-week-old WT, *Ercc1*$^{-/\Delta}$ and *Ercc1*$^{-/\Delta}$Atm$^{+/-}$mice (n=3 per genotype) probed for activation of ATM. GAPDH was used as a loading control. (**D**) Same liver lysates used to measure activation of NF-κB. (**E**) Fourteen-week-old livers from *Ercc1*$^{-/\Delta}$ and *Ercc1*$^{-/\Delta}$p65$^{+/-}$ mice (n=3 per genotype) were analyzed by western blot for activation of ATM (**F**) and NF-κB.

Persistent DNA damage-mediated DDR signaling, in particular ATM activation, has been demonstrated to be essential for the establishment of an NF-κB-dependent SASP phenotype in cell culture. Nuclear translocation of NEMO plays a critical role in relaying nuclear signal to cytoplasm to activate NF-κB in response to genotoxic stress [28]. For example, increased ATM phosphorylation and nuclear-localized NEMO were found in the *Zmpste24-/-* mouse model of Hutchinson-Gilford progeria syndrome (HGPS), where accumulation of nuclear prelamin-A leads to a perturbation of NF-κB signaling [34]. The transcription factor GATA4 was identified as a key mediator connecting DDR signaling to NF-κB activation and the senescent SASP phenotype [13]. In addition, ATM/IFI16 mediated non-canonical activation of DNA sensing adaptor STING was demonstrated recently in etoposide-induced nuclear DNA damage, leading to increased NF-κB activation [68]. However, in this study, we observed increased nuclear localization of NEMO in response to nuclear DNA damage, which could be ablated by an ATM inhibitor. Thus, our results support the presence of ATM/NEMO-dependent NF-κB pathway in response to chronic DNA damage.

ATM kinase is best known for its causal role in ataxia telangiectasia (AT), a rare autosomal recessive disease characterized by progressive neurodegeneration, immunodeficiency, cancer predisposition, radiosensitivity and premature skin aging [69–71]. Despite the fact that *Atm*-null mice have reduced dopaminergic neurons with age, decreased synaptic function in hippocampal neurons and defects in neuronal network activity, mice heterozygous for *Atm* improved not only neurodegenerative pathology, but also Huntington-like behavior in a mouse model of Huntington's disease [22, 72, 73]. In addition, genetic and/or pharmacologic reduction of ATM reduced doxorubicin-induced cardiotoxicity and rescued cardiac inflammation and heart failure caused by DNA single-strand breaks [74, 75]. These observations are consistent with our results showing neurologic symptoms and musculoskeletal pathology were improved in *Atm* haploinsufficient *Ercc1-/Δ* mice. In addition, our study showed that a short-term administration of KU55933 reduced multiple senescence and SASP markers in liver tissues in *Ercc1-/Δ* mice. These results indicate that ATM kinase may be a potential drug target for the treatment of multiple aging-related diseases, especially those
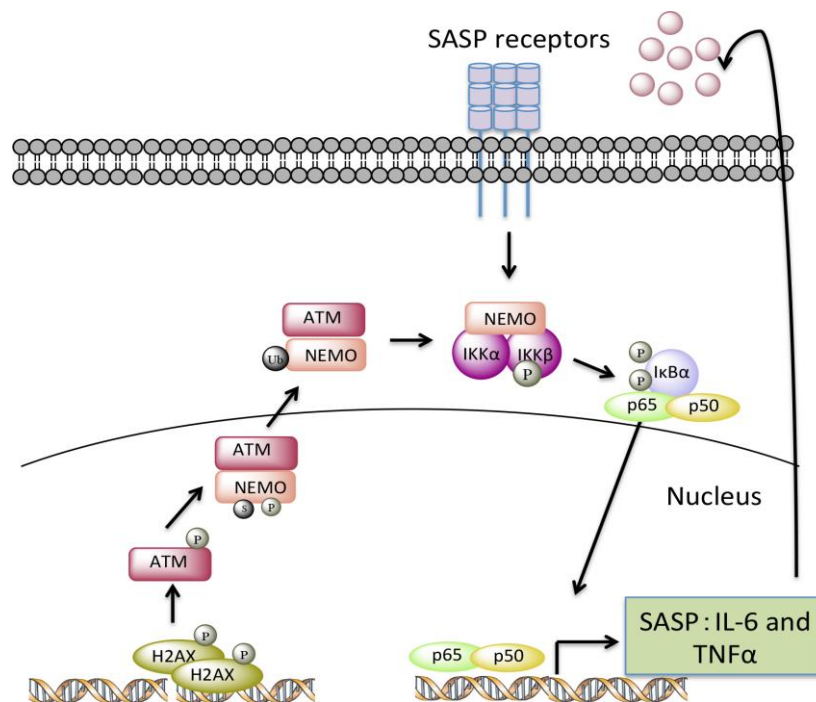

Figure 8. A model depicting how endogenous nuclear DNA damage activates NF-κB via an ATM- and NEMO-dependent mechanism to drive cellular senescence and senescence-associated secretory phenotype (SASP). In response to chronic accumulation of endogenous DNA damage, ATM undergoes autophosphorylation and promotes phosphorylation, SUMOylation, and monoubiquitylation of NEMO. As a result, monoubiquitylated NEMO along with ATM translocates to the cytoplasm, activating the IKK complex. Phosphorylation of IκB leads to the release of p65 so that it can translocate into nucleus upregulating a transcriptional program of certain SASP factors, such as TNFα and IL-6. Secreted SASP factors then trigger a second wave of NF-κB activation through cytokine receptors, further enhancing cell-autonomous pathway-mediated senescence and inducing non-cell-autonomous pathway-mediated senescence.

that have strong correlation with DNA damage accumulation. Given that heterozygous carriers of AT are symptom-free in general, we speculate that one WT allele of Atm is sufficient to exert its function in DNA repair and thereby doesn't trigger the neurological degeneration as seen in AT patients. Interestingly, studies in Chinese and Italian nonagenarians/centenarians have identified a single nucleotide polymorphism (SNP, rs189037) of in the promoter region of ATM that moderately represses transcription of *Atm* by regulating its binding to an activator protein 2α (AP-2α). These results suggest that, similar to our results in *Ercc1*$^{-/\Delta}$ mice, a slight reduction in ATM can contribute to extended lifespan in humans [76, 77].

Taken together, our results suggest that ATM acts as the main stimulus of NF-κB activation in DNA damaged-induced senescence and aging. Reduction in ATM either genetically or pharmacologically is able to reduce the adverse effects of chronic DNA damage, reducing cellular senescence, improving stem cell function and extending healthpsan. Thus, ATM and NF-κB represent therapeutic targets, at least later in life, for improving frailty and certain aging-related diseases.

MATERIALS AND METHODS

Cells and mice

Primary mouse embryonic fibroblasts (MEFs) were isolated on embryonic day 12.5-13.5. In brief, mouse embryos were isolated from yolk sac followed by removal of viscera, lung and heart. Embryos were then minced into fine chunks, covered with media, cultured at 3% oxygen to reduce stresses and serially passaged. MEFs were grown in 1:1 of Dulbecco's Modification of Eagles Medium (with 4.5 g/L glucose and L-glutamine) and Ham's F10 medium, supplemented with 10% fetal bovine serum, penicillin and streptomycin and non-essential amino acids. To induce oxidative stress and oxidative DNA damage, MEFs were switched to 20% oxygen at passage 3.

Ercc1$^{+/-}$ and *Ercc1*$^{+/\Delta}$ mice from C57BL/6J and FVB/NJ backgrounds were crossed to generate *Ercc1*$^{-/\Delta}$ F1 hybrid mice. *Atm*$^{+/-}$ mice were crossed to *Ercc1*$^{+/-}$ from C57BL/6J background to generate *Ercc1*$^{+/-}$*Atm*$^{+/-}$ mice, which were then bred with *Ercc1*$^{+/\Delta}$ mice from FVB/NJ background to generate F1 *Ercc1*$^{-/\Delta}$*Atm*$^{+/-}$ mice. Breeders were backcrossed for ten generations yielding F1 mice that are genetically identical. Animal protocols used in this study were approved by Scripps Florida Institutional Animal Care and Use Committee.

12-week-old *Ercc1*$^{-/\Delta}$ mice were injected intraperitoneally with 10 mg/kg of KU-55933 (AdooQ

Bioscience, Irvine, CA, USA) or the same volume of vehicle (1% DMSO: 30% PEG400: 69% H$_2$O) 3 times per week for two weeks. All mice were euthanized 1 hour after the last injection.

Immunoblotting

MEFs were treated with either KU-55933 (10 μM, Selleckchem) or vehicle for 72 hours prior to harvesting for analysis of protein expression. Cell lysates were prepared with RIPA buffer (20 mM Tris-HCl (pH 7.5), 150 mM NaCl, 1 mM Na$_2$EDTA, 1 μM EGTA, 1% NP-40, 1% sodium deoxycholate, 2.5 μM sodium pyrophosphate, 1 μM β-glycerophosphate, 1 μM Na$_3$VO$_4$ and 1 μg/ml leupeptin), supplemented with 1X of protease inhibitor cocktails (Sigma) and Halt phosphatase inhibitor cocktail (Thermo #78420). Snap-frozen liver and kidney samples were homogenized using FastPrep-24 instrument in RIPA buffer. Equal amounts of proteins (40 μg) were resolved on 4-15% Mini-PROTEAN TGX precast protein gels (Bio-Rad). Primary antibodies used are as follows: p-ATM Ser 1981 (cell lysates: Rockland cat. no. 200-301-400; tissue lysates: Santa Cruz sc-47739), ATM (CST #2873), p-KAP1 Ser 824(Abcam ab70369), KAP1 (Abcam ab22553), γ-H2AX (Novus NB100-384), PARP1 (CST #9532), p-p65 Ser 536 (CST #3033), p65 (CST #8242), p-IκBα Ser 32/36 (CST #9246), IκBα (Santa Cruz sc-371), p16^{INK4a} (Santa Cruz sc-1207), p21^{Cip1} (Santa Cruz sc-6246), LaminA/C (Santa Cruz sc-20681), anti-tubulin (CST #2146), and GAPDH (CST #5174). Blots were exposed to X-ray film in a dark room or developed on iBright™ FL1000 Imaging System (Figure 1E and 1F). Protein levels were quantified by Image J software.

Nuclear extraction

Extraction of cytoplasmic and nuclear fractions was performed using the NE-PER nuclear and cytoplasmic extraction reagents (Thermo Fisher) according to the manufacturer's instructions. Briefly, 1x10^6 cells were suspended and lysed in CERI and CERII reagents consecutively on ice to obtain cytoplasmic fractions. Pellets of intact nuclei were then suspended in NER reagent to release nuclear contents.

NF-κB luciferase reporter assay

Primary MEFs transfected with a NF-κB luciferase reporter construct were cultured in 6-well plates in triplicate in the absence or presence of KU-55933 (10 μM) for 72 hrs. Cells were then collected with Passive Lysis Buffer (Promega) and luciferase assay (Promega) was performed by using a luminometer according to the manufacturer's instructions.

Cell proliferation assay

Passage 3 MEFs were seeded at 5×10^5 cells in 10-cm plates, allowed to grow for 72-96 hours to reach confluence at 20% oxygen and then trypsinized for determination of cell number. Serial passage was carried until passage 5 and cell number was determined for each passage. Cell number was measured using a Moxi Z Mini automated cell counter. Log cell number was plotted versus passage number.

Enzyme-linked immunosorbent assay (ELISA)

Supernatant collected at the end of passage 4 from primary MEFs was analyzed for IL-6 production by ELISA using a mouse IL-6 ELISA kit (Becton Dickinson) according to the manufacturer's instructions.

Quantitative reverse transcription- polymerase chain reaction (qRT-PCR)

Snap-frozen tissues were preserved in RNAlater stabilization solution (Thermo Fisher). Total RNA was extracted using TRIZOL reagent (Life Technologies) and 1.5 µg of RNA was subjected to complementary DNA (cDNA) synthesis using SuperScript VILO cDNA synthesis kit (Thermo Fisher). qRT-PCR was performed with Platinum SYBR Green qPCR SuperMix-UDG with ROX (Thermo Fisher) in a StepOnePlus Real-Time PCR system. Relative expression of target genes was calculated using the comparative C_T method ($\Delta\Delta C_T$). ΔC_T was calculated by normalizing to an internal control gene *Actb* (β-actin) and $\Delta\Delta C_T$ by normalizing to the mean ΔC_T value of the control group. Primers used are as follows: *Cdkn1a* (p21^{Cip1}) forward: GTCAGGCTGGTCTGCCTCCG; *Cdkn1a* (p21^{Cip1}) reverse: CGGTCCCGTGGACAGTGAGCAG; *Cdkn2a* (p16^{INK4a}) forward: CCCAACGCCCCGAACT; *Cdkn2a* (p16^{INK4a}) reverse: GCAGAAGAGCTGCTACGTGAA; *Tnf* (TNF) forward: CTATGTCTCAGCCTCTTCTC; *Tnf* (TNF) reverse: CATTTGGGAACTTCTCATCC; *Il6* (IL-6) forward: AAGAAATGATGGATGCTACC; *Il6* (IL-6) reverse: GAGTTTCTGTATCTCTCTGAAG; *IL-1α* forward: ACGGCTGAGTTTCAGTGAGACC; *IL-1α* reverse: CACTCTGGTAGGTGTAAGGTGC; *IL-1β* forward: TGGACCTTCCAGGATGAGGACA; *IL-1β* reverse: GTTCATCTCGGAGCCTGTAGTG; *Mcp-1* forward: GCTACAAGAGGATCACCAGCAG; *Mcp-1* reverse: GTCTGGACCCATTCCTTCTTGG; *Pai-1* forward: CCTCTTCCACAAGTCTGATGGC; *Pai-1* reverse: GCAGTTCCACAACGTCATACTCG; *Cxcl-1* forward: TCCAGAGCTTGAAGGTGTTGCC; *Cxcl-1* reverse: AACCAAGGGAGCTTCAGGGTCA; *Cxcl-2* forward: CATCCAGAGCTTGAGTGTGACG; *Cxcl-2* reverse: GGCTTCAGGGTCAAGGCAAACT; *COX2* forward: GCGACATACTCAAGCAGGAGCA;

COX2 reverse: AGTGGTAACCGCTCAGGTGTTG; *iNOS* forward: GAGACAGGGAAGTCTGAAGCAC; *iNOS* reverse: CCAGCAGTAGTTGCTCCTCTTC; *p53* forward: CTCTCCCCCGCAAAAGAAAAA; *p53* reverse: CGGAACATCTCGAAGCGTTTA; *p19* forward: GGAGCTGGTGCATCCTGACGC; *p19* reverse: TGGCACCTTGCTTCAGGAGCTC; *Mmp3* forward: CTCTGGAACCTGAGACATCACC; *Mmp3* reverse: AGGAGTCCTGAGAGATTTGCGC; *Mmp12* forward: CACACTTCCCAGGAATCAAGCC; *Mmp12* reverse: TTTGGTGACACGACGGAACAGG; *Actb* (β-actin) forward: GATGTATGAAGGCTTTGGTC; *Actb* (β-actin) reverse: TGTGCACTTTTATTGGTCTC.

Immunofluorescent staining

Primary MEFs were seeded into 8-well chamber slides and allowed to attach overnight at 20% oxygen. Cells were then fixed with 4% paraformaldehyde (PFA) for 10 min, permeabilized with 0.3% Triton X-100 in PBS for 10 min and blocked with 3% BSA in PBST for 1 hr in room temperature. Primary antibody incubation was performed at 4°C overnight and secondary antibody incubation for 1 hr at room temperature. Primary antibodies used are as follows: anti-p65 (CST #8242) and anti-NEMO (Santa Cruz sc-8330). Cell nuclei were counterstained with Vectashield mounting medium with DAPI. Five images were acquired for each sample at 60x magnification using an Olympus confocal microscopy.

Senescence-associated β-galactosidase (SA-βgal) staining *in vitro* and *in vivo*

Primary MEFs were seeded into 6-well plates at 3×10^4 cells per well, allowed to attach overnight and then treated with either vehicle or KU-55933 at 10 µM for 72 hours. Fresh fat tissues were preserved in ice-cold PBS prior to staining. MEFs and adipose tissues were then fixed in 2% formaldehyde and 0.2% glutaraldehyde in PBS for 10 minutes followed by incubation with SA-βgal staining solution (MEFs: pH 5.8; Fat: pH 6.0; 40 µM citric acid in sodium phosphate buffer, 5 µM $K_4[Fe(CN)_6]$ $3H_2O$, 5 µM $K_3[Fe(CN)_6]$, 150 µM sodium chloride, 2 µM magnesium chloride and 1 mg/ml X-gal dissolved in N, N-dimethylformamide) for 16-20 hours in a 37°C incubator without CO_2 injector. To quantify, ten images were acquired randomly using a bright-field microscopy at 20x maginification. Total number of SA-βgal$^+$ cells was normalized to the total cell number (DAPI) to obtain the percentage of SA-βgal$^+$ cells.

Health evaluation

Health assessments were conducted weekly to assess the age at onset and severity of numerous age-related

conditions characteristic of Ercc1$^{-/\Delta}$ mice, including dystonia, ataxia, kyphosis, tremor, muscle wasting, spontaneous activity and coat condition. In addition, body weight and grip strength were measured. All aging symptoms were scored on a scale of 0, 0.5 and 1, except for dystonia on a scale from 0 to 5. The sum of aging scores was used to determine the overall health of the individual animals, then averaged by genotype and age group.

MDSPC isolation

The *Atm*$^{+/-}$, *Ercc1*$^{-/\Delta}$*Atm*$^{+/-}$ and *Ercc1*$^{-/\Delta}$ mice were sacrificed at 16 to 18 weeks of age, and MDSPC isolation was performed via a modified preplate technique as previously described [78, 79]. Briefly, the skeletal muscle tissue was minced and processed through a series of enzymatic dissociations: 0.2% of collagenase type XI (C7657, Sigma-Aldrich) for 1 hour, 2.4 units/ml of dispase (17105-041, Invitrogen) for 45 minutes, and 0.1% of trypsin-EDTA (15400-054, Invitrogen) for 30 minutes at 37°C. After enzymatic dissociation, the muscle cells were centrifuged and resuspended in proliferation medium (Dulbecco's modified Eagle's medium (DMEM, 11995-073, Invitrogen) supplemented with 10% fetal bovine serum (FBS, 10437-028, Invitrogen), 10% horse serum (HS, 26050-088, Invitrogen), 0.5% chicken embryo extract (CEE, CE650T-10, Accurate Chemical Co.), and 1% penicillin-streptomycin (15140-122, Invitrogen). The cells were then plated on collagen type I (C9791, Sigma-Aldrich) coated flasks. Different populations of muscle-derived cells were isolated based on their different adhesion characteristics. After 7 days, late preplate populations (slow-adhering cells), which have previously been described to contain the MDSPC fraction of cells, were obtained and cultured in proliferation medium [80].

MDSPC proliferation assay

MDSPCs were cultured at 5,000 cells per well in collagen-coated 24-well plates in proliferation medium. Cell proliferation was tested with an MTS assay. After 3 days, proliferation medium was removed from wells and 100 µl of fresh proliferation medium was added to each well and allowed to equilibrate for 1 hr. Then, 20 µl of MTS reagent (Promega, Cat# G3582) was added to each well and incubated for 4 hrs. The optical density at 490 nm was measured using a spectrophotometer.

Myogenic differentiation assay and fast myosin heavy chain staining

The cells were plated on 24 well plates (30,000 cells/well) in differentiation medium (DMEM supplemented with 2% FBS). Three days after plating, immunocytochemical staining for fast myosin heavy chain (MyHCf) was performed. Cells were fixed for 2 minutes in cold methanol (-20°C), blocked with 10% donkey serum (017-000-121, Jackson ImmunoResearch) for 1 hour and then incubated with a mouse anti-MyHCf (M4276, 1:250; Sigma-Aldrich) antibody for 2 hours at RT. The primary antibody was detected with an Alexa 594-conjugated anti-mouse IgG antibody (A21203, 1:500; Molecular probes) for 30 minutes. The nuclei were revealed by 4, 6-diamidino-2- phenylindole (DAPI, D9542, 100ng/ml, Sigma-Aldrich) staining. The percentage of differentiated myotubes was quantified as the number of nuclei in MyHCf positive myotubes relative to the total number of nuclei.

Histologic analysis

Tissues were fixed in 10% neutral buffered formalin (NBF) overnight before embedding in paraffin. 5 µm sections were acquired using a microtome. Hematoxylin and eosin (H&E) staining was conducted following a standard protocol.

Glycosaminoglycan (GAG) analysis

Snap frozen lumber spines were harvested at 12 weeks of age from Ercc1$^{-/\Delta}$ and Ercc1$^{-/\Delta}$Atm$^{+/-}$ mice. Nucleus pulposus (NP) tissue was isolated and dissected under a microscope and six lumbar intervertebral discs were pooled for analysis. GAG was isolated by papain digestion at 60°C for 2 hrs. Concentration of GAG was measured according to the 1,9-dimethymethylene blue (DMMB) procedure using chondroitin-6-sulfate (Sigma C-8529) as the standard. DNA concentration was measured using Pico Green assay (Molecular Probes). Fold change of GAG content was calculated by normalizing GAG to DNA concentration.

Micro-computed tomography

Micro-computed tomography (µCT) of spines isolated from 12-week-old wild type (WT), *Ercc1*$^{-/\Delta}$ and *Ercc1*$^{-/\Delta}$*Atm*$^{+/-}$ mouse littermates were acquired using the VivaCT 40 scanner (Scanco, Switzerland) with settings: energy 55 kvP, intensity 145 µA, integration time 200ms, isotropic voxel size 15 µm, threshold 235. 3D morphometric analysis were performed on lumbar vertebrae segments (L3-S1).

Statistical analysis

All values were presented as mean+/-S.E.M. Microsoft Excel and Graphpad Prism 6 were used for statistical analysis. Two-tailed Student's t-test was performed to determine differences between two groups. A value of p

<0.05 was considered as statistically significant, shown as *p <0.05, **p <0.01, and ***p < 0.001.

CONFLICTS OF INTEREST

The authors declare no conflicts of interest.

FUNDING

REFERENCES

1. Kirkwood TB. Understanding the odd science of aging. Cell. 2005; 120:437–47.
https://doi.org/10.1016/j.cell.2005.01.027
PMID:15734677

2. Baker DJ, Wijshake T, Tchkonia T, LeBrasseur NK, Childs BG, van de Sluis B, Kirkland JL, van Deursen JM. Clearance of p16Ink4a-positive senescent cells delays ageing-associated disorders. Nature. 2011; 479:232–36.
https://doi.org/10.1038/nature10600 PMID:22048312

3. Baker DJ, Childs BG, Durik M, Wijers ME, Sieben CJ, Zhong J, Saltness RA, Jeganathan KB, Verzosa GC, Pezeshki A, Khazaie K, Miller JD, van Deursen JM. Naturally occurring p16Ink4a-positive cells shorten healthy lifespan. Nature. 2016; 530:184–89.
https://doi.org/10.1038/nature16932 PMID:26840489

4. Chang J, Wang Y, Shao L, Laberge RM, Demaria M, Campisi J, Janakiraman K, Sharpless NE, Ding S, Feng W, Luo Y, Wang X, Aykin-Burns N, et al. Clearance of senescent cells by ABT263 rejuvenates aged hematopoietic stem cells in mice. Nat Med. 2016; 22:78–83.
https://doi.org/10.1038/nm.4010 PMID:26657143

5. Zhu Y, Tchkonia T, Pirtskhalava T, Gower AC, Ding H, Giorgadze N, Palmer AK, Ikeno Y, Hubbard GB, Lenburg M, O'Hara SP, LaRusso NF, Miller JD, et al. The Achilles' heel of senescent cells: from transcriptome to senolytic drugs. Aging Cell. 2015; 14:644–58.
https://doi.org/10.1111/acel.12344 PMID:25754370

6. Jun JI, Lau LF. The matricellular protein CCN1 induces fibroblast senescence and restricts fibrosis in cutaneous wound healing. Nat Cell Biol. 2010; 12:676–85.
https://doi.org/10.1038/ncb2070
PMID:20526329

7. Demaria M, Ohtani N, Youssef SA, Rodier F, Toussaint W, Mitchell JR, Laberge RM, Vijg J, Van Steeg H, Dollé ME, Hoeijmakers JH, de Bruin A, Hara E, Campisi J. An essential role for senescent cells in optimal wound healing through secretion of PDGF-AA. Dev Cell. 2014; 31:722–33.
https://doi.org/10.1016/j.devcel.2014.11.012
PMID:25499914

8. van Deursen JM. The role of senescent cells in ageing. Nature. 2014; 509:439–46.
https://doi.org/10.1038/nature13193 PMID:24848057

9. Storer M, Mas A, Robert-Moreno A, Pecoraro M, Ortells MC, Di Giacomo V, Yosef R, Pilpel N, Krizhanovsky V, Sharpe J, Keyes WM. Senescence is a developmental mechanism that contributes to embryonic growth and patterning. Cell. 2013; 155:1119–30.
https://doi.org/10.1016/j.cell.2013.10.041
PMID:24238961

10. Muñoz-Espín D, Cañamero M, Maraver A, Gómez-López G, Contreras J, Murillo-Cuesta S, Rodríguez-Baeza A, Varela-Nieto I, Ruberte J, Collado M, Serrano M. Programmed cell senescence during mammalian embryonic development. Cell. 2013; 155:1104–18.
https://doi.org/10.1016/j.cell.2013.10.019
PMID:24238962

11. Kuilman T, Peeper DS. Senescence-messaging secretome: SMS-ing cellular stress. Nat Rev Cancer. 2009; 9:81–94.
https://doi.org/10.1038/nrc2560
PMID:19132009

12. Coppé JP, Desprez PY, Krtolica A, Campisi J. The senescence-associated secretory phenotype: the dark side of tumor suppression. Annu Rev Pathol. 2010; 5:99–118.
https://doi.org/10.1146/annurev-pathol-121808-102144 PMID:20078217

13. Kang C, Xu Q, Martin TD, Li MZ, Demaria M, Aron L, Lu T, Yankner BA, Campisi J, Elledge SJ. The DNA damage response induces inflammation and senescence by inhibiting autophagy of GATA4. Science. 2015; 349:aaa5612.
https://doi.org/10.1126/science.aaa5612
PMID:26404840

14. Baar MP, Brandt RM, Putavet DA, Klein JD, Derks KW, Bourgeois BR, Stryeck S, Rijksen Y, van Willigenburg H, Feijtel DA, van der Pluijm I, Essers J, van Cappellen WA, et al. Targeted Apoptosis of Senescent Cells Restores Tissue Homeostasis in Response to Chemotoxicity and Aging. Cell. 2017; 169:132–147.e16.
https://doi.org/10.1016/j.cell.2017.02.031
PMID:28340339

15. Schafer MJ, White TA, Iijima K, Haak AJ, Ligresti G, Atkinson EJ, Oberg AL, Birch J, Salmonowicz H, Zhu Y, Mazula DL, Brooks RW, Fuhrmann-Stroissnigg H, et al. Cellular senescence mediates fibrotic pulmonary disease. Nat Commun. 2017; 8:14532. https://doi.org/10.1038/ncomms14532 PMID:28230051

16. Fuhrmann-Stroissnigg H, Ling YY, Zhao J, McGowan SJ, Zhu Y, Brooks RW, Grassi D, Gregg SQ, Stripay JL, Dorronsoro A, Corbo L, Tang P, Bukata C, et al. Identification of HSP90 inhibitors as a novel class of senolytics. Nat Commun. 2017; 8:422. https://doi.org/10.1038/s41467-017-00314-z PMID:28871086

17. Jeon OH, Kim C, Laberge RM, Demaria M, Rathod S, Vasserot AP, Chung JW, Kim DH, Poon Y, David N, Baker DJ, van Deursen JM, Campisi J, Elisseeff JH. Local clearance of senescent cells attenuates the development of post-traumatic osteoarthritis and creates a pro-regenerative environment. Nat Med. 2017; 23:775–81. https://doi.org/10.1038/nm.4324 PMID:28436958

18. Uziel T, Lerenthal Y, Moyal L, Andegeko Y, Mittelman L, Shiloh Y. Requirement of the MRN complex for ATM activation by DNA damage. EMBO J. 2003; 22:5612–21. https://doi.org/10.1093/emboj/cdg541 PMID:14532133

19. Guo Z, Kozlov S, Lavin MF, Person MD, Paull TT. ATM activation by oxidative stress. Science. 2010; 330:517–21. https://doi.org/10.1126/science.1192912 PMID:20966255

20. Lee JH, Paull TT. Direct activation of the ATM protein kinase by the Mre11/Rad50/Nbs1 complex. Science. 2004; 304:93–96. https://doi.org/10.1126/science.1091496 PMID:15064416

21. Lee JH, Paull TT. ATM activation by DNA double-strand breaks through the Mre11-Rad50-Nbs1 complex. Science. 2005; 308:551–54. https://doi.org/10.1126/science.1108297 PMID:15790808

22. Shiloh Y, Ziv Y. The ATM protein kinase: regulating the cellular response to genotoxic stress, and more. Nat Rev Mol Cell Biol. 2013; 14:197–210. https://doi.org/10.1038/nrm3546 PMID:23486281

23. Ditch S, Paull TT. The ATM protein kinase and cellular redox signaling: beyond the DNA damage response. Trends Biochem Sci. 2012; 37:15–22. https://doi.org/10.1016/j.tibs.2011.10.002 PMID:22079189

24. Soutoglou E, Misteli T. Activation of the cellular DNA damage response in the absence of DNA lesions. Science. 2008; 320:1507–10. https://doi.org/10.1126/science.1159051 PMID:18483401

25. Polo SE, Jackson SP. Dynamics of DNA damage response proteins at DNA breaks: a focus on protein modifications. Genes Dev. 2011; 25:409–33. https://doi.org/10.1101/gad.2021311 PMID:21363960

26. Perkins ND. Integrating cell-signalling pathways with NF-kappaB and IKK function. Nat Rev Mol Cell Biol. 2007; 8:49–62. https://doi.org/10.1038/nrm2083 PMID:17183360

27. Lee SJ, Dimtchev A, Lavin MF, Dritschilo A, Jung M. A novel ionizing radiation-induced signaling pathway that activates the transcription factor NF-kappaB. Oncogene. 1998; 17:1821–26. https://doi.org/10.1038/sj.onc.1202088 PMID:9778048

28. Wu ZH, Shi Y, Tibbetts RS, Miyamoto S. Molecular linkage between the kinase ATM and NF-kappaB signaling in response to genotoxic stimuli. Science. 2006; 311:1141–46. https://doi.org/10.1126/science.1121513 PMID:16497931

29. McCool KW, Miyamoto S. DNA damage-dependent NF-κB activation: NEMO turns nuclear signaling inside out. Immunol Rev. 2012; 246:311–26. https://doi.org/10.1111/j.1600-065X.2012.01101.x PMID:22435563

30. Biton S, Ashkenazi A. NEMO and RIP1 control cell fate in response to extensive DNA damage via TNF-α feedforward signaling. Cell. 2011; 145:92–103. https://doi.org/10.1016/j.cell.2011.02.023 PMID:21458669

31. Korhonen P, Helenius M, Salminen A. Age-related changes in the regulation of transcription factor NF-κ B in rat brain. Neurosci Lett. 1997; 225:61–64. https://doi.org/10.1016/S0304-3940(97)00190-0 PMID:9143018

32. Brégégère F, Milner Y, Friguet B. The ubiquitin-proteasome system at the crossroads of stress-response and ageing pathways: a handle for skin care? Ageing Res Rev. 2006; 5:60–90. https://doi.org/10.1016/j.arr.2005.09.002 PMID:16330259

33. Helenius M, Hänninen M, Lehtinen SK, Salminen A. Changes associated with aging and replicative senescence in the regulation of transcription factor nuclear factor-kappa B. Biochem J. 1996; 318:603–08. https://doi.org/10.1042/bj3180603 PMID:8809053

34. Osorio FG, Bárcena C, Soria-Valles C, Ramsay AJ, de Carlos F, Cobo J, Fueyo A, Freije JM, López-Otín C. Nuclear lamina defects cause ATM-dependent NF-κB activation and link accelerated aging to a systemic inflammatory response. Genes Dev. 2012; 26:2311–24. https://doi.org/10.1101/gad.197954.112 PMID:23019125

35. Tilstra JS, Robinson AR, Wang J, Gregg SQ, Clauson CL, Reay DP, Nasto LA, St Croix CM, Usas A, Vo N, Huard J, Clemens PR, Stolz DB, et al. NF-κB inhibition delays DNA damage-induced senescence and aging in mice. J Clin Invest. 2012; 122:2601–12. https://doi.org/10.1172/JCI45785 PMID:22706308

36. Chien Y, Scuoppo C, Wang X, Fang X, Balgley B, Bolden JE, Premsrirut P, Luo W, Chicas A, Lee CS, Kogan SC, Lowe SW. Control of the senescence-associated secretory phenotype by NF-κB promotes senescence and enhances chemosensitivity. Genes Dev. 2011; 25:2125–36. https://doi.org/10.1101/gad.17276711 PMID:21979375

37. Adler AS, Sinha S, Kawahara TL, Zhang JY, Segal E, Chang HY. Motif module map reveals enforcement of aging by continual NF-kappaB activity. Genes Dev. 2007; 21:3244–57. https://doi.org/10.1101/gad.1588507 PMID:18055696

38. Bernal GM, Wahlstrom JS, Crawley CD, Cahill KE, Pytel P, Liang H, Kang S, Weichselbaum RR, Yamini B. Loss of Nfkb1 leads to early onset aging. Aging (Albany NY). 2014; 6:931–43. https://doi.org/10.18632/aging.100702 PMID:25553648

39. Oakley F, Mann J, Nailard S, Smart DE, Mungalsingh N, Constandinou C, Ali S, Wilson SJ, Millward-Sadler H, Iredale JP, Mann DA. Nuclear factor-kappaB1 (p50) limits the inflammatory and fibrogenic responses to chronic injury. Am J Pathol. 2005; 166:695–708. https://doi.org/10.1016/S0002-9440(10)62291-2 PMID:15743782

40. Lu ZY, Yu SP, Wei JF, Wei L. Age-related neural degeneration in nuclear-factor kappaB p50 knockout mice. Neuroscience. 2006; 139:965–78. https://doi.org/10.1016/j.neuroscience.2005.12.062 PMID:16533569

41. Jurk D, Wilson C, Passos JF, Oakley F, Correia-Melo C, Greaves L, Saretzki G, Fox C, Lawless C, Anderson R, Hewitt G, Pender SL, Fullard N, et al. Chronic inflammation induces telomere dysfunction and accelerates ageing in mice. Nat Commun. 2014; 2:4172. https://doi.org/10.1038/ncomms5172 PMID:24960204

42. Tilstra JS, Clauson CL, Niedernhofer LJ, Robbins PD. NF-κB in Aging and Disease. Aging Dis. 2011; 2:449–65. PMID:22396894

43. Chung HY, Cesari M, Anton S, Marzetti E, Giovannini S, Seo AY, Carter C, Yu BP, Leeuwenburgh C. Molecular inflammation: underpinnings of aging and age-related diseases. Ageing Res Rev. 2009; 8:18–30. https://doi.org/10.1016/j.arr.2008.07.002 PMID:18692159

44. Wang J, Clauson CL, Robbins PD, Niedernhofer LJ, Wang Y. The oxidative DNA lesions 8,5'-cyclopurines accumulate with aging in a tissue-specific manner. Aging Cell. 2012; 11:714–16. https://doi.org/10.1111/j.1474-9726.2012.00828.x PMID:22530741

45. Sedelnikova OA, Horikawa I, Zimonjic DB, Popescu NC, Bonner WM, Barrett JC. Senescing human cells and ageing mice accumulate DNA lesions with unrepairable double-strand breaks. Nat Cell Biol. 2004; 6:168–70. https://doi.org/10.1038/ncb1095 PMID:14755273

46. Rodier F, Coppé JP, Patil CK, Hoeijmakers WA, Muñoz DP, Raza SR, Freund A, Campeau E, Davalos AR, Campisi J. Persistent DNA damage signalling triggers senescence-associated inflammatory cytokine secretion. Nat Cell Biol. 2009; 11:973–79. https://doi.org/10.1038/ncb1909 PMID:19597488

47. Coppé JP, Rodier F, Patil CK, Freund A, Desprez PY, Campisi J. Tumor suppressor and aging biomarker p16(INK4a) induces cellular senescence without the associated inflammatory secretory phenotype. J Biol Chem. 2011; 286:36396–403. https://doi.org/10.1074/jbc.M111.257071 PMID:21880712

48. Gurkar AU, Niedernhofer LJ. Comparison of mice with accelerated aging caused by distinct mechanisms. Exp Gerontol. 2015; 68:43–50. https://doi.org/10.1016/j.exger.2015.01.045 PMID:25617508

49. Wang C, Jurk D, Maddick M, Nelson G, Martin-Ruiz C, von Zglinicki T. DNA damage response and cellular senescence in tissues of aging mice. Aging Cell. 2009; 8:311–23. https://doi.org/10.1111/j.1474-9726.2009.00481.x PMID:19627270

50. Hickson I, Zhao Y, Richardson CJ, Green SJ, Martin NM, Orr AI, Reaper PM, Jackson SP, Curtin NJ, Smith GC. Identification and characterization of a novel and specific inhibitor of the ataxia-telangiectasia mutated kinase ATM. Cancer Res. 2004; 64:9152–59. https://doi.org/10.1158/0008-5472.CAN-04-2727 PMID:15604286

51. Fang EF, Scheibye-Knudsen M, Brace LE, Kassahun H, SenGupta T, Nilsen H, Mitchell JR, Croteau DL, Bohr VA. Defective mitophagy in XPA via PARP-1 hyperactivation and NAD(+)/SIRT1 reduction. Cell. 2014; 157:882–96. https://doi.org/10.1016/j.cell.2014.03.026 PMID:24813611

52. Sharpless NE, DePinho RA. How stem cells age and why this makes us grow old. Nat Rev Mol Cell Biol. 2007; 8:703–13. https://doi.org/10.1038/nrm2241 PMID:17717515

53. Lavasani M, Robinson AR, Lu A, Song M, Feduska JM, Ahani B, Tilstra JS, Feldman CH, Robbins PD, Niedernhofer LJ, Huard J. Muscle-derived stem/progenitor cell dysfunction limits healthspan and lifespan in a murine progeria model. Nat Commun. 2012; 3:608. https://doi.org/10.1038/ncomms1611 PMID:22215083

54. Ladiges W, Snyder JM, Wilkinson E, Imai DM, Snider T, Ge X, Ciol M, Pettan-Brewer C, Pillai SPS, Morton J, Quarles E, Rabinovitch P, Niedernhofer L, Liggitt D. A New Preclinical Paradigm for Testing Anti-Aging Therapeutics. J Gerontol A Biol Sci Med Sci. 2017; 72:760–62. https://doi.org/10.1093/gerona/glx019 PMID:28329081

55. Urban JP, Winlove CP. Pathophysiology of the intervertebral disc and the challenges for MRI. J Magn Reson Imaging. 2007; 25:419–32. https://doi.org/10.1002/jmri.20874 PMID:17260404

56. Saar G, Zhang B, Ling W, Regatte RR, Navon G, Jerschow A. Assessment of glycosaminoglycan concentration changes in the intervertebral disc via chemical exchange saturation transfer. NMR Biomed. 2012; 25:255–61. https://doi.org/10.1002/nbm.1741 PMID:22253087

57. Guerin HA, Elliott DM. Chapter 3: Structure and Properties of Soft Tissues in the Spine. In: Kurtz SM, Edidin AA, editors. Spine Technology Handbook. Burlington: Academic Press; 2006. pp. 35–62. https://doi.org/10.1016/B978-012369390-7/50004-6

58. Vo N, Seo HY, Robinson A, Sowa G, Bentley D, Taylor L, Studer R, Usas A, Huard J, Alber S, Watkins SC, Lee J, Coehlo P, et al. Accelerated aging of intervertebral discs in a mouse model of progeria. J Orthop Res. 2010; 28:1600–07. https://doi.org/10.1002/jor.21153 PMID:20973062

59. Beg AA, Sha WC, Bronson RT, Ghosh S, Baltimore D. Embryonic lethality and liver degeneration in mice lacking the RelA component of NF-kappa B. Nature. 1995; 376:167–70. https://doi.org/10.1038/376167a0 PMID:7603567

60. Hertlein E, Wang J, Ladner KJ, Bakkar N, Guttridge DC. RelA/p65 regulation of IkappaBbeta. Mol Cell Biol. 2005; 25:4956–68. https://doi.org/10.1128/MCB.25.12.4956-4968.2005 PMID:15923614

61. Collado M, Blasco MA, Serrano M. Cellular senescence in cancer and aging. Cell. 2007; 130:223–33. https://doi.org/10.1016/j.cell.2007.07.003 PMID:17662938

62. Hasty P, Campisi J, Hoeijmakers J, van Steeg H, Vijg J. Aging and genome maintenance: lessons from the mouse? Science. 2003; 299:1355–59. https://doi.org/10.1126/science.1079161 PMID:12610296

63. Anson RM, Bohr VA. Mitochondria, oxidative DNA damage, and aging. J Am Aging Assoc. 2000; 23:199–218. https://doi.org/10.1007/s11357-000-0020-y PMID:23604866

64. Ames BN. Endogenous oxidative DNA damage, aging, and cancer. Free Radic Res Commun. 1989; 7:121–28. https://doi.org/10.3109/10715768909087933 PMID:2684796

65. Rodier F, Muñoz DP, Teachenor R, Chu V, Le O, Bhaumik D, Coppé JP, Campeau E, Beauséjour CM, Kim SH, Davalos AR, Campisi J. DNA-SCARS: distinct nuclear structures that sustain damage-induced senescence growth arrest and inflammatory cytokine secretion. J Cell Sci. 2011; 124:68–81. https://doi.org/10.1242/jcs.071340 PMID:21118958

66. Nelson G, Wordsworth J, Wang C, Jurk D, Lawless C, Martin-Ruiz C, von Zglinicki T. A senescent cell bystander effect: senescence-induced senescence. Aging Cell. 2012; 11:345–49. https://doi.org/10.1111/j.1474-9726.2012.00795.x PMID:22321662

67. Choudhury AR, Ju Z, Djojosubroto MW, Schienke A, Lechel A, Schaetzlein S, Jiang H, Stepczynska A, Wang C, Buer J, Lee HW, von Zglinicki T, Ganser A, et al. Cdkn1a deletion improves stem cell function and lifespan of mice with dysfunctional telomeres without accelerating cancer formation. Nat Genet. 2007; 39:99–105. https://doi.org/10.1038/ng1937 PMID:17143283

68. Dunphy G, Flannery SM, Almine JF, Connolly DJ, Paulus C, Jønsson KL, Jakobsen MR, Nevels MM, Bowie AG, Unterholzner L. Non-canonical Activation of the DNA Sensing Adaptor STING by ATM and IFI16 Mediates NF-κB Signaling after Nuclear DNA Damage. Mol Cell. 2018; 71:745–760.e5. https://doi.org/10.1016/j.molcel.2018.07.034 PMID:30193098

69. Angèle S, Romestaing P, Moullan N, Vuillaume M, Chapot B, Friesen M, Jongmans W, Cox DG, Pisani P, Gérard JP, Hall J. ATMHaplotypes and Cellular Response to DNA Damage. Cancer Res. 2003; 63:8717–25. PMID:14695186

70. McKinnon PJ. ATM and ataxia telangiectasia. EMBO Rep. 2004; 5:772–76. https://doi.org/10.1038/sj.embor.7400210 PMID:15289825

71. McKinnon PJ. ATM and the molecular pathogenesis of ataxia telangiectasia. Annu Rev Pathol. 2012; 7:303–21. https://doi.org/10.1146/annurev-pathol-011811-132509 PMID:22035194

72. Lu XH, Mattis VB, Wang N, Al-Ramahi I, van den Berg N, Fratantoni SA, Waldvogel H, Greiner E, Osmand A, Elzein K, Xiao J, Dijkstra S, de Pril R, et al. Targeting ATM ameliorates mutant Huntingtin toxicity in cell and animal models of Huntington's disease. Sci Transl Med. 2014; 6:268ra178. https://doi.org/10.1126/scitranslmed.3010523 PMID:25540325

73. Eilam R, Peter Y, Groner Y, Segal M. Late degeneration of nigro-striatal neurons in ATM-/- mice. Neuroscience. 2003; 121:83–98. https://doi.org/10.1016/S0306-4522(03)00322-1 PMID:12946702

74. Zhan H, Aizawa K, Sun J, Tomida S, Otsu K, Conway SJ, Mckinnon PJ, Manabe I, Komuro I, Miyagawa K, Nagai R, Suzuki T. Ataxia telangiectasia mutated in cardiac fibroblasts regulates doxorubicin-induced cardiotoxicity. Cardiovasc Res. 2016; 110:85–95. https://doi.org/10.1093/cvr/cvw032 PMID:26862121

75. Higo T, Naito AT, Sumida T, Shibamoto M, Okada K, Nomura S, Nakagawa A, Yamaguchi T, Sakai T, Hashimoto A, Kuramoto Y, Ito M, Hikoso S, Akazawa H, Lee JK, Shiojima I, McKinnon PJ, Sakata Y, Komuro I. DNA single-strand break-induced DNA damage response causes heart failure. Nat Commun. 2017; 8:15104. https://doi.org/10.1038/ncomms15104 PMID:28436431

76. Chen T, Dong B, Lu Z, Tian B, Zhang J, Zhou J, Wu H, Zhang Y, Wu J, Lin P, Zhang J, Xu H, Mo X. A functional single nucleotide polymorphism in promoter of ATM is associated with longevity. Mech Ageing Dev. 2010; 131:636–40. https://doi.org/10.1016/j.mad.2010.08.009 PMID:20816691

77. Piaceri I, Bagnoli S, Tedde A, Sorbi S, Nacmias B. Ataxia-telangiectasia mutated (ATM) genetic variant in Italian centenarians. Neurol Sci. 2013; 34:573–75. https://doi.org/10.1007/s10072-012-1188-5 PMID:22960875

78. Lavasani M, Lu A, Thompson SD, Robbins PD, Huard J, Niedernhofer LJ. Isolation of muscle-derived stem/progenitor cells based on adhesion characteristics to collagen-coated surfaces. Methods Mol Biol. 2013; 976:53–65. https://doi.org/10.1007/978-1-62703-317-6_5 PMID:23400434

79. Gharaibeh B, Lu A, Tebbets J, Zheng B, Feduska J, Crisan M, Péault B, Cummins J, Huard J. Isolation of a slowly adhering cell fraction containing stem cells from murine skeletal muscle by the preplate technique. Nat Protoc. 2008; 3:1501–09. https://doi.org/10.1038/nprot.2008.142 PMID:18772878

80. Qu-Petersen Z, Deasy B, Jankowski R, Ikezawa M, Cummins J, Pruchnic R, Mytinger J, Cao B, Gates C, Wernig A, Huard J. Identification of a novel population of muscle stem cells in mice: potential for muscle regeneration. J Cell Biol. 2002; 157:851–64. https://doi.org/10.1083/jcb.200108150 PMID:12021255

SUPPLEMENTARY MATERIALS

Supplementary Figures
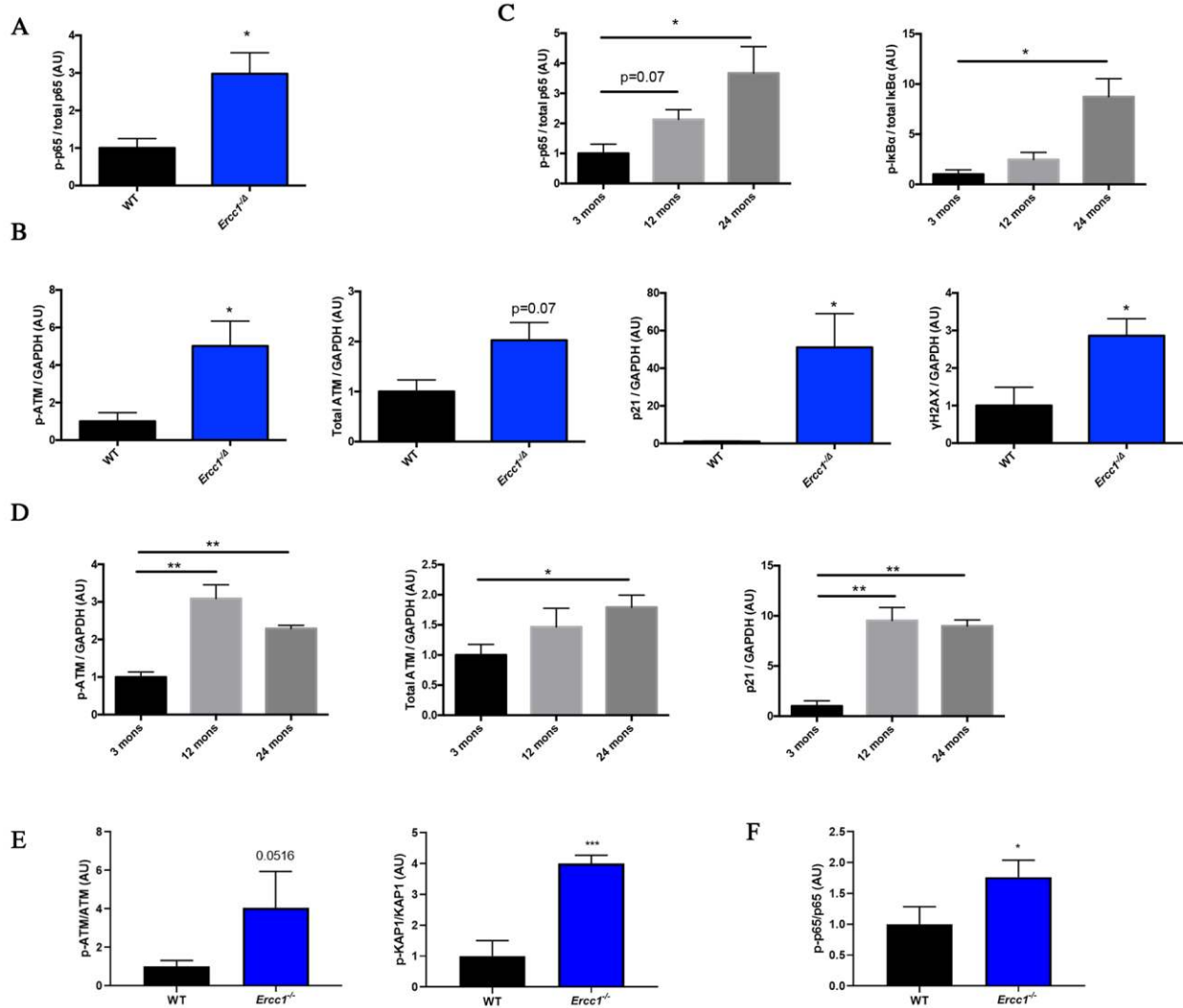
Supplementary Figure 1. DDR and NF-κB are activated in tissues from progeroid *Ercc1*$^{-/\Delta}$ and old WT mice. Densitometric analysis of Western Blot shown in Figure 1A (**A**), Figure 1B (**B**), Figure 1C. (**C**) and Figure 1D (**D**). (**A–B**) Two-tailed Student's t-test was performed. (**C–D**) One-way ANOVA was performed. *p <0.05, **p <0.01 or as indicated in the figure.
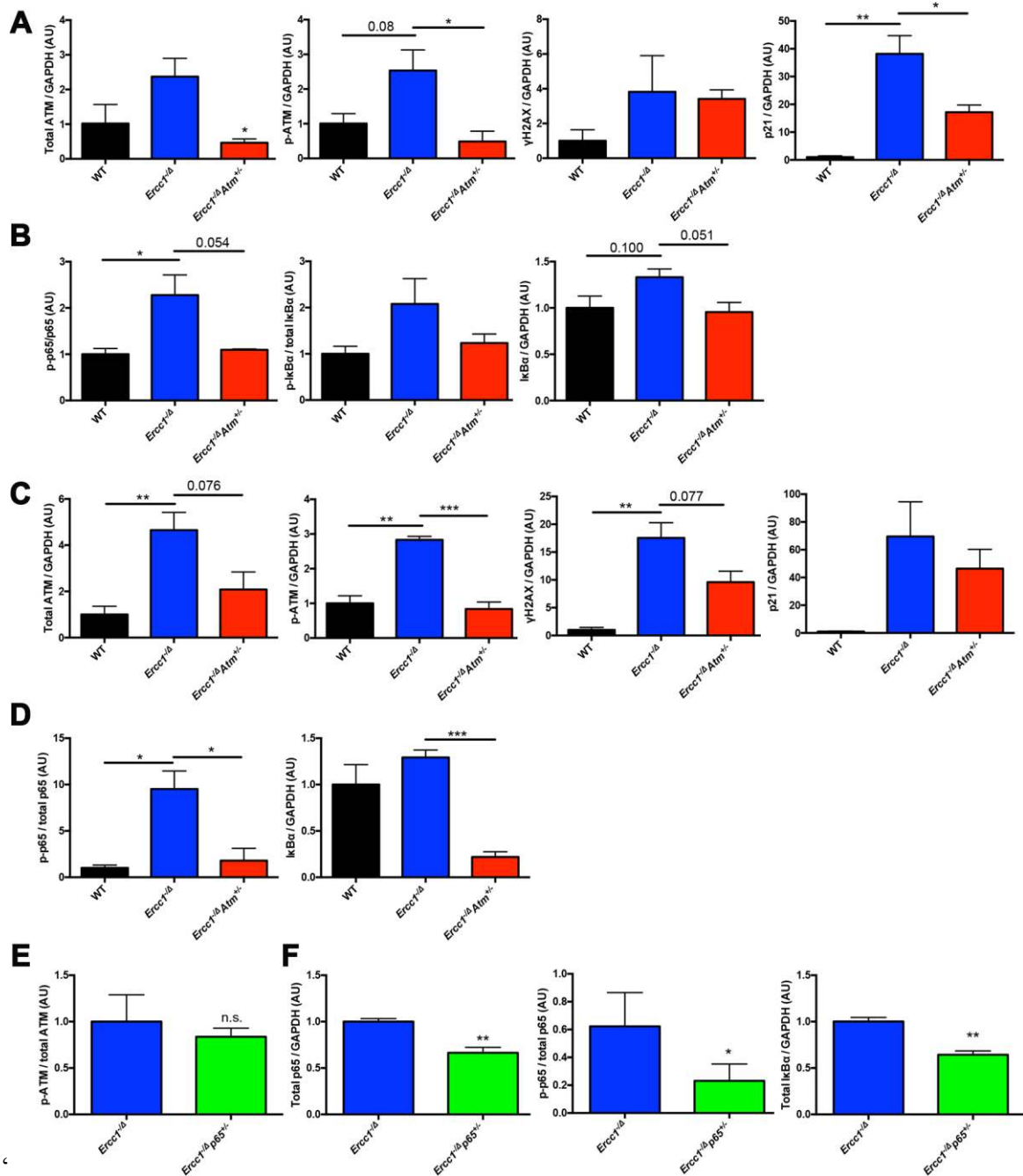
Supplementary Figure 2. Atm haploinsufficiency reduces senescence by regulating NF-κB activation. Densitometric analysis of Western Blot shown in Figure 7A (**A**), Figure 7B (**B**), Figure 7C (**C**), Figure 7D (**D**), Figure 7E (**E**) and Figure 7F (**F**). P values were determined using a Student's t-test. *p <0.05, **p <0.01, ***p<0.001 or as indicated in the figure.
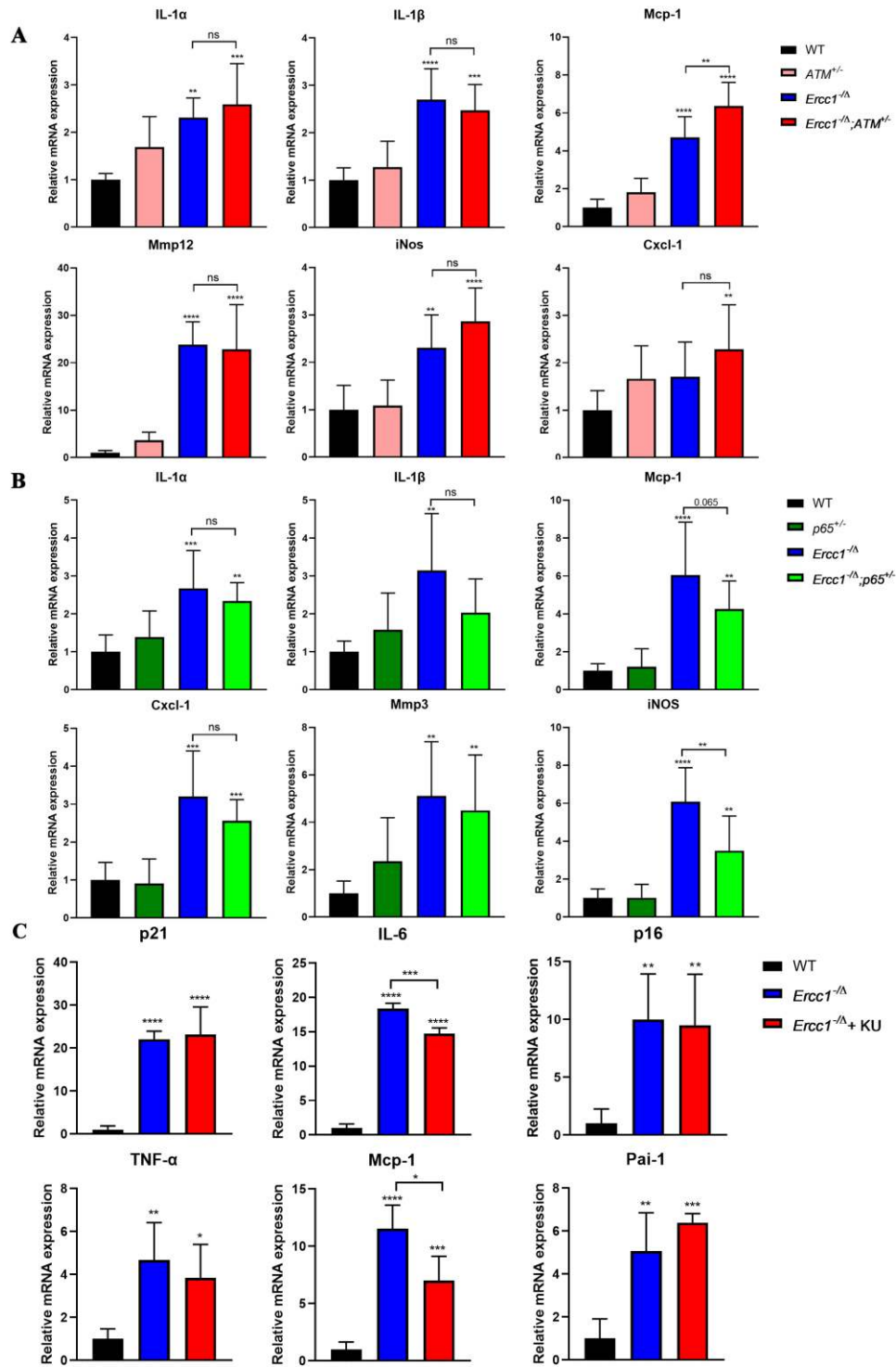
Supplementary Figure 3. Genetic reduction or pharmacologic inhibition of *Atm* or *NF-κB* attenuates aging phenotypes and reduces cellular senescence *in vivo*. (**A**) qRT-PCR analysis of mRNA expression in liver from 12-week-old WT, *Atm*+/-, *Ercc1*-/Δ and *Ercc1*-/Δ*Atm*+/- mice. n=3-6 per group. (**B**) qRT-PCR analysis of mRNA expression in liver from 10 to 12-week-old WT, *p65*+/-, *Ercc1*-/Δ and *Ercc1*-/Δp65+/- mice. n=4-5 per group. (**C**) mRNA expression of senescence markers in the kidney of 12-week-old *Ercc1*-/Δ mice treated with 10 mg/kg of KU-55933 intraperitoneally 3 times per week for two weeks. n = 3 per group. Graphs represent mean+/- s.e.m. P value was determined using Student's t-test. *p<0.05, **p<0.01, ***p <0.001, ****p <0.0001.